Materials Advances

ROYAL SOCIETY OF CHEMISTRY

REVIEW

View Article Online
View Journal | View Issue

Cite this: *Mater. Adv.*, 2022, 3, 1874

Microfluidic sensors based on two-dimensional materials for chemical and biological assessments

Sithara Radhakrishnan,† Minu Mathew† and Chandra Sekhar Rout *

Received 7th October 2021,
Accepted 11th January 2022

DOI: 10.1039/d1ma00929j

rsc.li/materials-advances

There has been an exponential increase in the number of studies of two-dimensional (2D) layered materials for sensing applications since the isolation of graphene in 2004. These materials serve as a supporting substrate and an active sensing element in a variety of health care and environmental applications due to their exceptional and frequently tunable physical, optical, electrical, and electrochemical capabilities. Microfluidic sensors are a relatively new technology that shows promise in health care and environmental applications due to quick response, inexpensive and highly sensitive analysis with high yield. Due to their appealing electrical and electrochemical properties with a variety of structural features and fabrication processes, 2D materials are a good contender for microfluidic sensor applications. As a result, these two-dimensional material-based microfluidic devices can provide a well-controlled microenvironment for both low-cost point-of-care analytics and advanced chemical/biological analysis. Different 2D materials for microfluidic sensors and their possible use in various health care and environmental applications including wearable sensors are critically addressed in this review. Finally, the challenges and prospects for the future of 2D materials in terms of commercial challenges and long-term sustainability are examined.

1. Introduction

Sensors are electrical devices that typically offer concurrent information on the system's composition by connecting the recognition element to a transducer.[1] A perfect sensor would have the highest possible throughput, user-friendly selectivity, and sensitivity, capable of in-field operation, and affordable in cost. It should also meet the world health organization's standards for portable sensors.[2] Microfluidic devices, from these perspectives, are fascinating technologies for accomplishing Lab-on-a-Chip (LOC)-based point-of-care applications.[3] Sensors employed in a microfluidic platform are referred to as "Microfluidic Sensors." Microfluidics is an entirely new

Centre for Nano and Material Science, Jain University, Jain Global Campus, Jakkasandra, Ramanagara, Bangalore-562112, India. E-mail: csrout@gmail.com, r.chandrasekhar@jainuniversity.ac.in

† S. R. and M. M. contributed equally.

Sithara Radhakrishnan

Ms Sithara Radhakrishnan received her BTech in Polymer engineering from Mahatma Gandhi University (Kerala, India) in 2016 and MTech in Polymer engineering from Cochin University of Science and Technology (Kerala, India) in 2018. She is currently a Nano-science doctoral student at the Centre for Nano & Material Science, Jain University, working under Prof. Dr Chandra Sekhar Rout. Her current research focuses on designing and fabrication of 2D material nanocomposite for energy storage applications.

Minu Mathew

Ms Minu Mathew is a JRF in Chemistry at the Centre for Nano and Material Science (CNMS), Jain University, Bangalore under the supervision of Prof. Chandra Sekhar Rout. She received her MPhil in Chemistry from the Christ University, Bangalore in 2019. She completed her Master's (2014) and Bachelor's (2012) degree in Chemistry from the Mahatma Gandhi University, Kottayam, Kerala, India. Her research interests include synthesis and characterization of two dimensional (2D) materials for energy and environment related applications.

field that manipulates fluids in channels as small as tens of micrometers in diameter.[4] The key advantages of these microfluidic systems include regulated liquid flow, minimal reagent and sample use, rapid analysis, system compactness and parallelization, reduced waste generation, along disposability.[5,6] Previously, microfluidics was primarily concerned with incorporating microsensors with fluidic elements (pumps, actuators and valves, so on) and the miniaturization of analytical assays. Micro-fabricated structures were then used to create Micro Total Analysis Systems (μTAS) and LOC. The significant difference between these two was explained by Gupta *et al.*, where μTAS refers to integrating the entire sequence of lab procedures to perform chemical analysis. In contrast, LOC refers to integrating one or more lab processes onto a single chip.[7]

Chandra Sekhar Rout

Prof. Chandra Sekhar Rout is a full Professor at Centre for Nano & Material Sciences (CNMS), Jain University. Before joining CNMS, He was a DST-Ramanujan Fellow at IIT Bhubaneswar, India (2013–2017). He received his BSc (2001) and MSc (2003) degrees from Utkal University and his PhD from JNCASR, Bangalore (2008) under the supervision of Prof. C. N. R. Rao, Bharat Ratna. He did his postdoctoral research at National University of Singapore (2008–2009), Purdue University, USA (2010–2012) and UNIST, South Korea (2012–2013). He was awarded the prestigious Ramanujan Fellowship and Young Scientist award of Department of Science and Technology, Govt. of India in 2013, emerging investigator award 2017 from Elsevier, IAAM medal 2017 from International Association of Advanced Materials 2017, Young researcher award from Venus International Foundation in 2015. His research interests include preparation and characterization of 2D layered materials and its hybrids for chemical sensors and biosensors, supercapacitors and energy storage devices, field emitters and electronic devices. He has authored more than 180 research papers in international journals and edited 3 books. His current h-index is 44 with total citations ~9000. He was ranked top 2% scientists in India by the Stanford study in 2019 and 2020. He serves as board members of various reputed journals and is associate editor of "RSC Advances" a journal of Royal Society of Chemistry and "American Journal of Engineering and Applied Sciences" of Science Publications. He has completed several sponsored projects funded by government of India and supervised PhD, postdocs and MSc students. He has delivered more than fifty invited talks in various national and international conferences and travelled to several countries such as USA, UK, Israel, Singapore, South Korea, Brazil and Russia etc. for collaboration purposes.

A range of life science areas, including cell biology, genetic studies, and protein analysis, have benefited from the miniaturization of these microfluidic devices.[8] Current research is focused on the creation of sensors for microscale measurement. These devices are now primarily used in various fields of study, including biology, biomedical sciences, chemistry, and engineering.[9,10] Microfluidic devices are not only small but may also be used as a platform for analysis systems. Combining the extraordinary features of nanomaterials with microfluidic sensors improves selectivity and sensitivity and has stimulated interest in a broad range of applications. Nanomaterials have a lot of potential in the field because of their biocompatibility, catalytic efficiency, quantum size effect, electrical conductivity, Raman spectrum effect, reactivity, surface and interface effects, and other features of microfluidic sensors.[11,12] Nanomaterials can be used to support nanostructure electrodes or act as signal enhancers, labels, and label supports in microfluidic sensors.[10] Among these gold and platinum nanoparticles are frequently used as electrodes in microfluidic sensors. Main drawbacks of metal nanoparticles are their small potential window and fouling/passivation produced by contact with materials. Compared to metal nanoparticles, carbon nanomaterials-based electrodes are more stable over a wide potential range and less prone to fouling.[13] Carbon nanomaterials, including carbon nanohorns (CNHs), carbon nanotubes (CNT) and carbon nanospheres (CNSs), have already been proven tremendous success in microfluidic sensors.[10] Among these CNTs have received the most significant attention due to their exceptional mechanical and electrochemical properties and high thermal and electrical conductivity. However still, their one-dimensional (1D) nature poses a significant problem during fabrication.[14] Alternatively. graphene derivatives are gaining popularity among these carbon nanomaterials due to the higher adhesion offered by its flat 2D shape and greater availability of active sites.[10] Graphene's unique and exotic features include its ultra-light honey comb structure with a planar density of roughly 0.77 mg m^{-2} and super thinness (0.35 nm). Because of these features, graphene has piqued the interest of many researchers in the manufacture of microfluidic sensors, and its applications have already been addressed by Chen *et al.*, Sengupta *et al.*, and others.[5,15] Inspired by these graphene-based microfluidic sensors in 2015, Yang *et al.*, for the very first time, fabricated a microfluidic sensor using MoS_2 for fluorescent DNA detection.[16] MXene, a novel material recently added to the 2D material family, may also help overcome existing microfluidic sensors issues. This material, which has excellent biocompatibility as well as outstanding electrical conductivity, is ideal for microfluidic sensors.[17] The importance of all these 2D materials in microfluidic sensors is shown in Fig. 1.

Biosensors are advancing due to breakthroughs advancements in manufacturing processes and device integration; according to Frost & Sullivan, the global biosensor industry is poised to increase at a compound annual growth rate (CAGR)of 12 percent from $17.7 billion in 2018 to $31.2 billion by the end of 2023, up from $17.7 billion in 2018.[18] Given their immense potential for sensing applications, it's shocking that two-dimensional (2D)

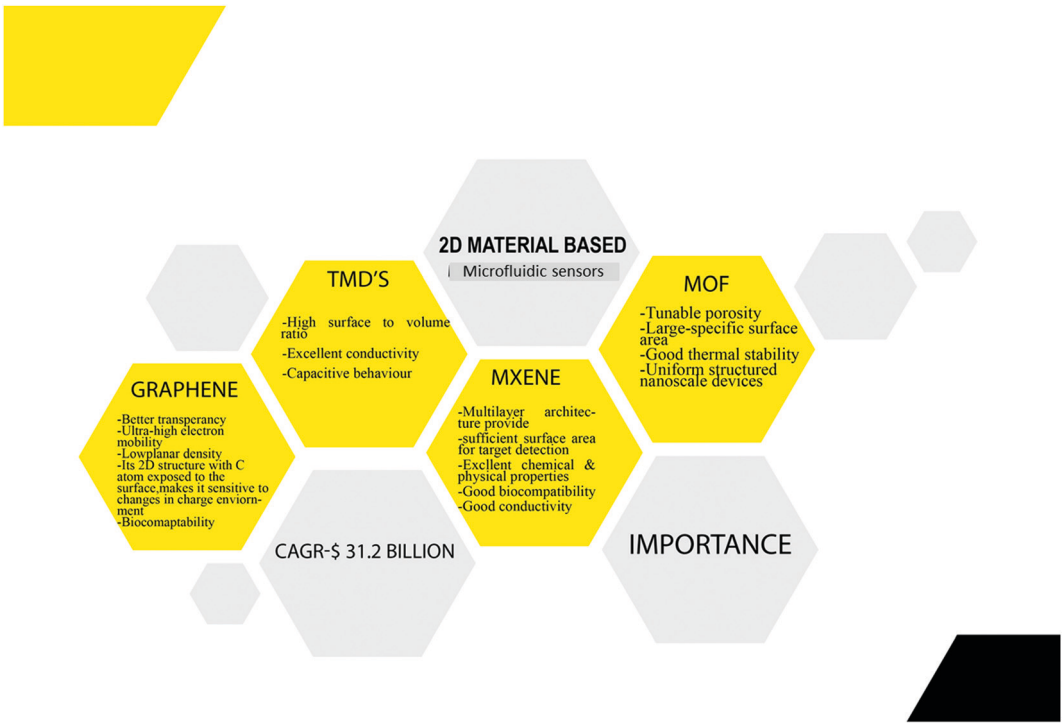

Fig. 1 Importance of 2D materials in microfluidic sensors.

materials are still neglected in the field of microfluidic sensors. Although various publications have detailed the most recent achievements of graphene-based microfluidic sensors and LOD for detecting a broad spectrum of analytes from biomolecules to gases and water pollutants, more research is needed.[5,12,15] Further research is required despite recent improvements in graphene-based LOD and microfluidic sensors for detecting a wide range of analytes, including biomolecules, gases, and water pollutants. To the best of our knowledge, there is no comprehensive literature review report on the application of 2D material-based microfluidic sensors and their capacity to detect a broad range of analytes.

Furthermore, MXene, TMD, and MOF-based microfluidic sensors are new, with no comprehensive review study available. As a result, a current review concentrating on 2D nanomaterial microfluidic sensors is needed to highlight the advantages of 2D nanomaterial-based microfluidic sensors and to provide ideas for further increasing sensor performance/fabrication for real-world applications. Current breakthroughs in graphene, TMD, MXene, and MOF-based microfluidic sensors will be discussed in this review, with a focus on biomolecule, water and gas pollutant detection. Quick and low-concentration detection using 2D microfluidic sensors are the most appealing advantages of microfluidic sensors. They enable early contaminant detection, early disease diagnosis, and steady environmental monitoring, as well as time savings for routine low-concentration examination. We also look at the benefits and drawbacks of 2D nanomaterial microfluidic sensors and provide recommendations for future studies in this area. We make a concerted effort to emphasize the most important work that may be found using Google Scholar, SciFinder, Web of Science and Scopus. In this

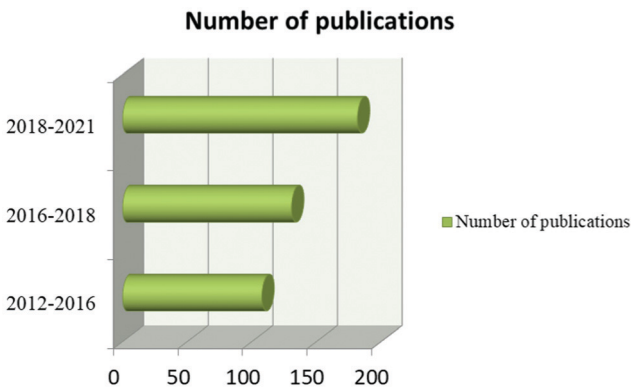

Fig. 2 Number of papers published in 2D material-based microfluidic sensors.

case, a literature search was conducted using the Scopus database and the keywords "microfluidic sensor" and "graphene + TMD + MXene + MOF" to select papers for review. The number of articles published in 2D material-based microfluidic sensors is shown in Fig. 2.

1.1 Why 2D materials?

In 2007, Pokropivny and Skorokhod classified nanomaterials into 0D, 1D, 2D and 3D based on their confinement.[19,20] Compared to other nanomaterials, two-dimensional materials have numerous advantages which makes them highly desirable for their application in microfluidic sensors. Firstly, they have high surface–area-to-volume ratio, enabling a wide range of interactions between two-dimensional material and analytes.[21]

This enhanced interaction property was utilized to design and develop sensors for the quantitative detection of alkali, gas, and heavy metals to biologically relevant molecules (*e.g.*, lactate, glucose, DNA and protein).[20,22] Further, the high surface to volume ratio property imparts some additional benefits, including greater amount of active sites,and easy surface functionalization. Secondly, 2D materials exhibit a broad spectrum of conductivity, which can be further fine-tuned by configuration and morphology engineering, enabling effective signal transduction *via* a molecular binding event.[23] Additionally, dimensionality engineering methodology can be adopted to tune the inherent characteristics of the 2D materials, such as their fluorescence, conductivity, reactivity, and magnetic permeability.[20] Aside from the above mentioned benefits 2D nanomaterials are advantageous in terms of their device integration compatibility.[24] Especially, they have excellent compatibility with the existing ultra-thin silicone channel technology, while the integration of the device in 0D materials is difficult, it is challenging to develop electrical contacts with 1D materials and miniature devices with 3D materials.[25] Finally, we believe that for future generation microfluidic sensors: the below mentioned properties of 2D materials will be highly beneficial (1) atomically thin two-dimensional material nanosheets offer a greater surface area due to the full surface exposure of the atoms; (2) comparing the basal plane of two-dimensional materials edge sites is chemically more reactive; and the open space of van der Waals allows electrolyte intercalation and (3) with their flexibility and robust laminar structure, 2D materials could be easily integrated into microfluidic beds and flexible wearable sensors.[22,26]

1.2 Fabrication of microfluidc devices

The methodologies usually employed for the manufacturing of microfluidic sensors can be split into two major groups: top-down and bottom-up. Top-down involves large-scale patterning and reduction of lateral dimensions to the nanoscale. Top-down approaches are further subdivided into three types (i) surface machining (ii) film/bulk machining and (iii) mold-machining. Bottom-up techniques use highly regulated chemical reactions to arrange atoms or molecules to form nanostructures. Table 1 summarizes the advantages and disadvantages of these fabrication strategies.

1.3 Detection principles of microfluidic sensors

The large-scale integration of numerous microfluidic components, such as micropumps, microfluidic mixers, microchannels, microvalves and other elements to handle and regulate fluids at the microscale, is involved in integrated microfluidic devices.[27] They are widely employed in biological, chemical, and medicinal research. There have already been numerous thoughtful review articles on related topics.[27–30]

In the realm of chemical, biological diagnosis, or analysis on microfluidic devices, various detection methods are available. Microfluidic detection methods are divided into three categories: mass spectrometry methods,[31–33] electrochemical[34–36] and optical methods.[29,37,38] Because of their selectivity and sensitivity, electrochemical and optical approaches are the most commonly used. In addition to the basic technologies mentioned above, methodologies such as acoustical,[39,40] nuclear magnetic resonance (NMR)[41,42] spectroscopy and magneto-resistive[43] are being combined with microfluidics for sensing applications. As shown in Fig. 3, the common optical detection methods include direct detection by detecting light properties such as absorbance,[44] luminescence[45–47] and fluorescence[48–50]-based approaches, as well as light property modulation detections like surface plasmon resonance (SPR) detection.[51–53] These techniques often include evanescent waves,[54] fibre optics,[30] interferometry,[55–57] Raman spectroscopy,[58,59] SPR and optical waveguides.[30]

Electrochemical measurements, which are typically used to detect electroactive species, are based on electrical property modifications of analyte species that undergo redox reactions. There are three types of measurements: amperometries,[60–62] conductometry[63,64] and potentiometry measures.[65] The principles of these methods was already been reviewed.

Mass spectrometry (MS) is capable of performing extremely selective detection by tracking the route of ions in magnetic and/or electric fields, revealing the ions' mass and charge.[66]

Table 1 Fabrication techniques of microfluidic sensors

Fabrication techniques	Advantages	Disadvantages
Chemical wet etching	Simple process, cheap, high selectivity with controllable etching rate	Chemical contamination, orientation dependant, under cutting and poor repetability
Plasma etching	High reproducablilty, easy to control, high feature resolution and no liquid chemical waste	Poor selectivity, high cost, potential radiation damage
Soft lithography	Low cost, ability to manufacture 3D geometries, and great resolution (down to a few nm)[206]	Pattern distortion, prone to defect[206]
Optical lithography/ conventional photolithography	Microscale features benefit from high wafer throughputs[207]	Typically, a smooth surface is required to begin with, with chemical post-treatment required[207]
Injection molding	Complex geometry, fine details, and 3D geometries are simple to produce, with a low cycle time, large production, and high automation[208]	Exclusively used for thermoplastics, expensive mould, difficult to produce huge undercut shapes[208]
Hot embossing	Microstructure replication that is cost-effective, precise, and quick, as well as mass production[209]	Complex 3D structures are difficult to construct since they are limited to thermoplastics[209]
Laser photoablation	Large format production, rapid[210]	Limited materials, multiple treatment sessions[210]

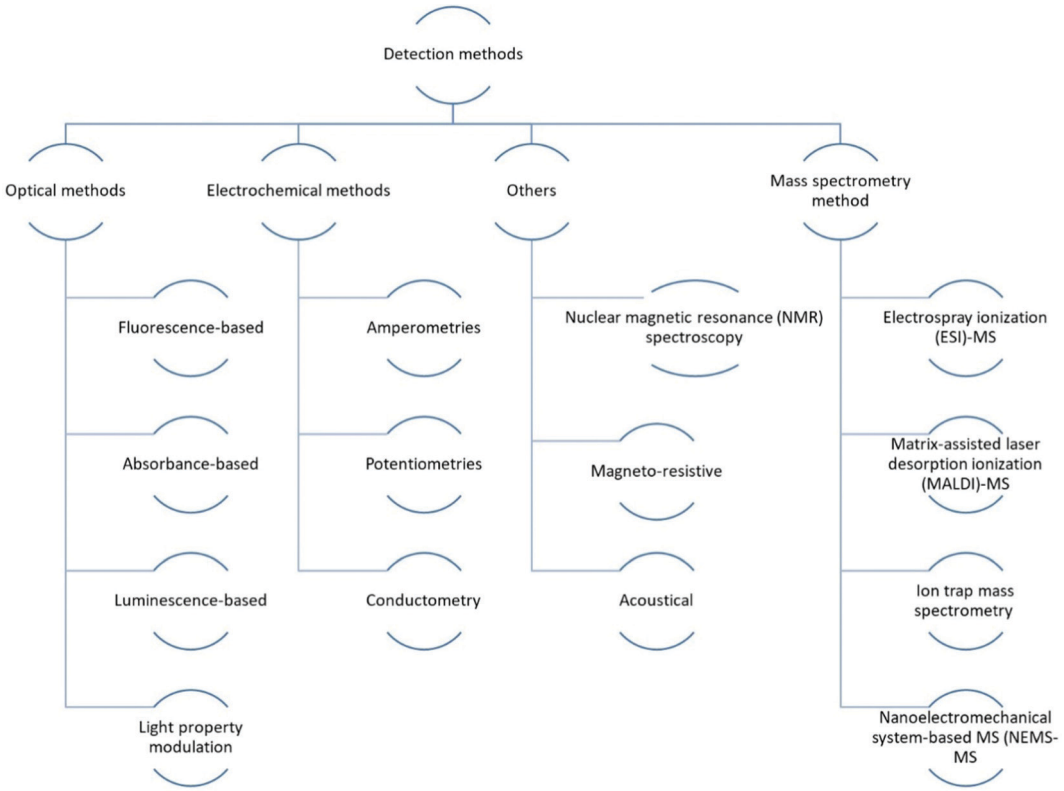

Fig. 3 Detection principles of microfluidic sensors.

Its major application is in proteomic investigations for protein separation and identification based on protein fragmentation patterns. There are two methods for identifying following separation. The first method is direct detection, which involves searching through the database utilising the different types of proteins obtained. Tandem MS is a more complex method for obtaining protein fragments/ions for sequence tagging.[67] For this application, numerous MS configurations[30,68,69] have already been designed to connect with microfluidic devices which is shown in Fig. 3.

Other approaches, such as NMR spectroscopy, have been investigated for use in microfluidic detection in addition to the three basic categories. It is a well-developed detection approach in life sciences and chemistry that makes use of the magnetic characteristics of nuclei, as well as chemical shift Knight shift and/or the Zeeman effect, for detection. Biological and chemical analyte species such as proteins and nucleic acids can be detected using NMR spectroscopy. However, the low sensitivity of standard NMR detection techniques has limited its employment in microscale systems. Despite the technological obstacles, NMR remains a viable alternative to optical or electrochemical technologies for microfluidic applications: It does not have the problem of optical accessibility for the ROI, and the data acquisition time is substantially quicker, making time-resolved studies more easier; it has superior detection pervasiveness than electrochemical approaches, which are limited to electroactive substances. As a result, resolving the weak NMR signal problem in microsystems, whether by signal augmentation or better detection instrumentation, will open the door to a wider range of NMR lab-on-a-chip applications.[30]

1.4 Applications of microfluidic sensors

Microfluidic sensors have been widely used in various life science and medical detection reserach and applications. There have already been numerous thoughtful review articles on related topics. Gao *et al.* summarised the applications of microfluidic chip technology in food safety sensing.[70] Its application in biomedical field was reviewd by Pattanayak *et al.*[71] also in the field of environmental analysis was summarized by Zhang *et al.*[72] Microfluidic sensors also allow for the creation of quick, sensitive, and portable diagnostic tools, allowing for the rapid and accurate identification of a wide range of infections and its application in pathogen sensing was reviewed by Marihofer *et al.*[73]

2. Graphene-based microfluidic sensors

Due to its outstanding sensitivity to electronic disruptions when target species (biological, gas or chemical) interact, graphene is now being researched and developed as biological, physical, and chemical electronic sensors for targets such as different biological agents, chemical species, and gases. The ever-increasing usage of sensors in society and the growing demand for devices with the following characteristics: high performance, low power consumption and cost, which is crucial

for portable or distant applications, has motivated these research endeavors.[74–76] The effectiveness of sensing instruments is highly dependent on the materials used and the design concepts used. Graphene has enormous potential as a sensor material for applications such as LOD, point-of-care, environmental, and industrial monitoring in this regard. Indeed, it has been proposed that graphene technology could develop low-cost, compact sensors with previously unimagined capabilities.[77] The advantages of graphene-based microfluidic sensors include rapid diagnosis, real-time detection, low-cost, multi-target analysis, automation, small sample volume, and higher selectivity and sensitivity.[78] So far, there have been numerous reviews of graphene-based microfluidic devices. In 2018, Chen *et al.* published the first review of graphene-based microfluidic devices for different applications such as contaminant detection, virus and bacteria detection, glucose and protein detection, and sensor applications. However, research on graphene-based microfluidic sensors and LOD is still in its early stages, despite predictions that the point-of-care application will be a hot topic.[79] Chaudhery Mustansar Hussain and Joydip Sengupta published a review on graphene-based LOD devices the following year, attempting to provide insight into point-of-care devices as well. This paper examines the critical applications of graphene-based microfluidics, including everything from detecting chemical food pollutants to detecting retinal electrical signals and even early stage cancer diagnosis, as well as the fabrication method for graphene-based LOCs (2). In the same year M. Materón *et al.* discussed about graphene based microfluidic and chip devices for detection of biomolecules.[78] Wu *et al.* published a review on graphene-based microfluidic sensors in 2020, which includes graphene-based microfluidic FET sensors, optical sensors, and biosensors for chemical and biomolecular detection.[80] Microfluidic sensors based on graphene can be classified according to applications, such as chemical and biological analysis and other applications. Biological applications are further subdivided into those used for diagnostic purposes and those used for biomolecule detection.

2.1 Graphene-based microfluidic biosensors

Graphene and its oxidized counterparts (such as GO, rGO, and others) have become critical nanomaterials in the domain of biosensors, notably in the construction of low-cost optoelectronic devices, due to their unique optoelectronic capabilities. The research purpose of combining microfluidic technology in biosensing is to implement additional miniaturized devices capable of high selectivity and sensitivity, small throughput, fast response and automated testing. The potential benefits such as portability and high-throughput analysis are realized by combining microfluidic technology and biosensing, resulting in intelligent real-time detection. Graphene nanomaterials could be used to functionalize and recognize a variety of biological analytes because biomolecules come in a variety of sizes.[80,81]

2.1.1 For cancer detection. The gold standard for tumor identification, confirmation, and classification is still solid tissue biopsies, which involve the removal of tumor tissue and subsequent cytological and histopathological examination. In any case, the procedure is excruciatingly painful and intrusive which can also result in Inflammation, bleeding, and the spread of cancerous cells. Furthermore, the number of samples collected is insufficient in most cases. Because of tumor tissue's spatial and temporal heterogeneity, the results may be inconclusive.[82,83] On the other hand, tumor tissues shed various components into the body fluids, including cells, exosomes, proteins and nucleic acids, which could serve as tumor biomarkers that provide information similar to tissue biopsies.[84] The current biomarkers for cancer detection were tabulated by Choi *et al.*[85] Although these fluid biopsies can be taken from any biological fluid, blood is the most commonly used because it can detect almost all cancer types. In contrast, saliva or urine can only detect specific types. Despite this, identifying biomarkers in small quantities using blood samples is difficult due to diverse cells and chemicals. As a result, the advancement of sensitive systems for detecting and analyzing low concentrations of biomarkers in body fluids is a way to facilitate personalized medicine for cancer treatment.[84] Although microfluidic technologies have a lot of potentials, combining them with two-dimensional graphene improves the sensitivity and selectivity of microfluidic sensors and can help detect cancer biomarkers. In 2012, Cao *et al.* published the first graphene oxide (GO) based Förster resonance energy transfer (FRET) microfluidic chip for cancer cell detection. Because the aptamer-based microfluidic chip was not producing enough signals, they were inspired to develop this FRET aptasensing microfluidic device, which takes advantage of graphene's fluorescence quenching and DNA adsorption abilities. This FRET on biosensing microfluidic chips was an excellent choice for detecting cancer cells, and the aptamer immobilization and washing steps could be eliminated. This GO-enhanced microfluidic technology is the first graphene-based microfluidic sensor with significant sensitivity and selectivity for cancer cell detection.[86] Soon after these studies, Wu *et al.* developed microfluidic paper-based electrochemical immunodevices to detect cancer biomarkers using a signal amplification strategy obtained by incorporating graphene, HRP, and antibody co-immobilized silica nanoparticles.[87] Although several publications and review papers based on graphene and graphene derivatives-based microfluidic devices for cancer detection are available, we are only discussing recent papers, *i.e.*, those published between 2020 and 2021.

Wu *et al.* investigated a high-performance microfluidic sensor for the early detection of ovarian cancer. This microfluidic sensor is fabricated with a GO-assembled substrate that helps immobilize the antibody where the large surface area property of graphene results in enhanced immobilization of capture antibodies. They designed a microfluidic chip with multiple parallel channels shown in Fig. 4a and a microprinted capture antibody barcode above the detection substrate (Fig. 4b). This captured antibody barcode was then printed over GO substrate. The sample loading chip is made of microwells (Fig. 4c). Each microwell covers an entire array of the capture antibody barcode, allowing the immobilized antibodies to capture all ten biomarkers in the sample material. The biomarker antigen is then

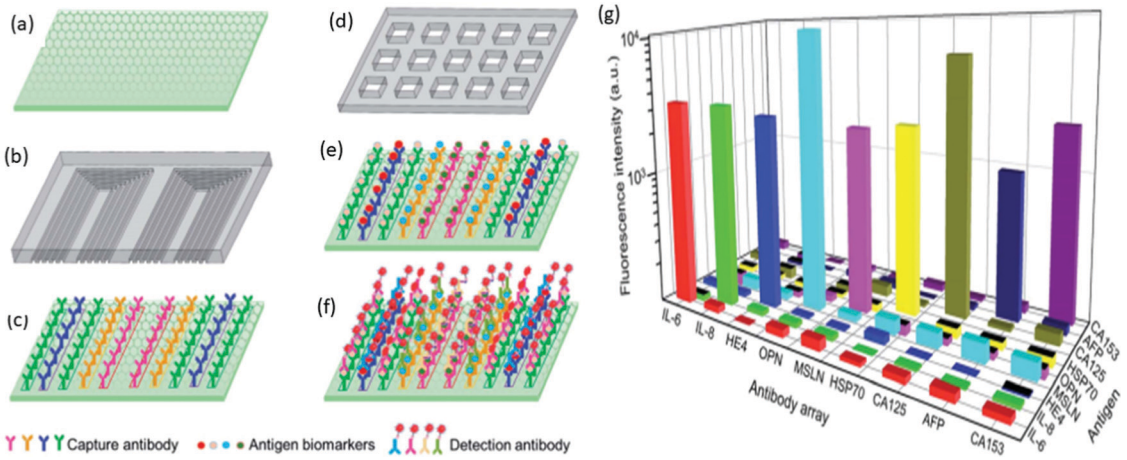

Fig. 4 (a) Substrate for the detection of ovarian cancer biomarker (b) chip was microprinted (c) antibody capturing by the barcode which was printed on the substrate (d) sample filling chip (e) biomarker antigens caught by antibody barcode (f) fluorescence labeling for detection of biomarkers (g) detection specificity of the prepared chip. Source: reprinted from Y. Wu, C. Wang, P. Wang, C. Wang, Y. Zhang and L. Han, A high-performance microfluidic detection platform to conduct a novel multiple-biomarker panel for ovarian cancer screening, *RSC Adv.*, 2021, **11**(14), 8124–8133.

incubated for 10 minutes with the immobilized antibody before the fluorescence-labeled detection is specifically conjugated with the antigen, as shown in Fig. 4d and e. This microfluidic sensor was able to detect all of the traditional ovarian cancer indicators and inflammatory factors with an ultra-low detection limit of roughly 0.01 μ mL^{-1} and 1 pg mL^{-1}. As a result, this microfluidic sensor can detect ovarian cancer at an early stage. These antibodies all have a specific reaction with the respective biomarkers in the detection chip. As shown in Fig. 4g, coupled antigen–antibody pairs have significantly higher fluorescence intensity than mismatched pairs.[88] Niu *et al.* reported using an antibody-functionalized GO lab-on-chip device to isolate and analyze circulating tumor cells (CTC) from the bladder of cancer patients. They employed a GO chip coated with a biotinylated anti-EpCAM and anti-EGFR antibody mixture to capture CTCs from whole blood. Immunofluorescence staining for cytokeratin (cancer cell marker), DAPI (nuclei), EGFR and HER2 (invasive phenotype markers), and CD45 (white blood cell marker) were used to count CTCs in patient samples. CTCs were defined as cells with a DAPI + CK + CD45-phenotype.[89]

A growing amount of attention is being paid to combining the appealing qualities of aptamers with the particular benefits of electrochemical detection technique. Electrochemistry gives new avenues for integrating aptamer interactions with the signal-generating component, allowing for speedy, low-cost protein diagnostics.[90] As a result, an electrochemical approach for detecting EGFR was created. Using these advantages of the electrochemical detecting technique, Wang *et al.* built an origami-paper-device using graphene nanocomposite. Wax printing was used to generate the device's hydrophilic and hydrophobic regions, which define fluid channels. On the other hand, the electrochemical electrodes were created using screen printing (shown in Fig. 5a). By simply folding the paper to allow valving or flow, the system facilitated sample processing and detection. Thionine (THI)/amino-functionalized graphene (NH_2–GO)/gold particle (AuNP) nanocomposites were fabricated as working electrodes (WE) also immobilize aptamers *via* Au–S bonds (Fig. 5b). Here the amino-functionalized graphene exhibited a corrugated structure and thus resulted in enhanced surface area of the electrode; hence they can load a large amount of TFI molecule and AuNP. They presynthesized thiol-modified anti-EGFR aptamers and used a simple electrochemical detection approach that did not require tagging of either antigen or aptamer. For EGFR, this suggested aptasensor has a LOD of around 5 pg mL^{-1} and a linear range of 0.05 to 200 ng mL^{-1}. The electrochemical response was shown to be lower when the EGFR aptamer was immobilized on the electrode surface compared to graphene-modified electrodes (Fig. 5c). Insulating aptamers appear to have hampered electron transport, resulting in a reduction in current responsiveness. More insulating immunocomplexes would form with a greater concentration of antigens, resulting in a decreased electrochemical current. The CV analysis showed that the electrochemical paper-based aptasensor could be constructed and operated satisfactorily. Electron transport appears to have been impeded by insulating aptamers, resulting in a decrease in current responsiveness. Also, more insulating immunocomplexes would form with a higher concentration of antigens, resulting in a lower electrochemical current. The CV results demonstrated that the electrochemical paper-based aptasensor was successfully manufactured and functioned. Similar results were obtained from DPV, where the modified electrode showed a DPV response with a peak current of roughly 16.99 μA, which was lowered to 14.98 μA after aptamer immobilization. This suggested aptasensor unites low-cost paper-based microfluidic devices with an electrochemical detection approach that is extremely sensitive. The origami approach streamlined the device even more and reduced sample consumption.[91] Another paper-based electrochemical sensor for the early quantitative detection of pancreatic cancer was recently published by Prasad *et al.* Pancreatic ductal adenocarcinoma (PDAC) is another significant cancer killer. People with PDAC have higher levels

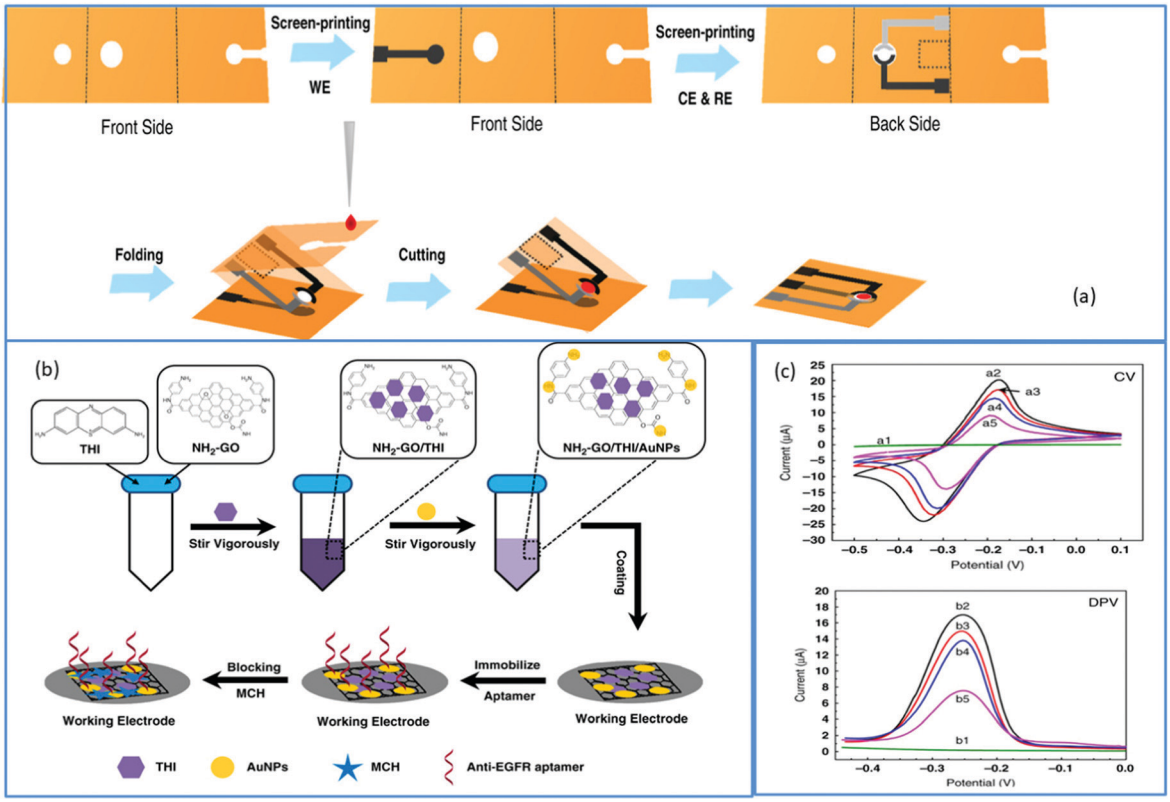

Fig. 5 (a) Fabrication procedure of origami paper-based sensor (b) modification process (c) CV and DPV response of the fabricated sensor. Source: reprinted from Y. Wang, S. Sun, J. Luo, Y. Xiong, T. Ming, J. Liu, *et al.*, Low sample volume origami-paper-based graphene-modified aptasensors for label-free electrochemical detection of cancer biomarker-EGFR, *Microsyst. Nanoeng.*, 2020, **18**, 6(1), 1–9.

of PEAK1 protein expression than healthy people. A cheap, disposable, unique yet straightforward paper-based electrochemical immunosensor was created to trace the PDAC biomarker PEAK1 using a standard sandwich-type immunoassay. They developed this sensor over paper-based electrodes using a stencil printing technique. Then GO was simply drop cast over paper-based electrodes for covalent modification to incorporate the capturing antibody (Anti-PEAK1). This immunosensing device uses gold nanoparticle (AuNPs)-tagged Anti-PEAK1 bioprobes to detect PEAK1. With a LOD of around 10 pg mL^{-1}, this sensor displayed remarkable sensitivity during PEAK1 detection.[92] Torul *et al.* recently developed another paper-based electrochemical sensor based on gold nanoparticle/graphene and Au nanoparticle/MoS_2 for the selective and sensitive identification of miRNA-155 and miRNA-21, which are the most significantly altered miRNAs in the majority of cancer types. Torul *et al.* constructed (Fig. 6a) the hydrophobic barriers of this paper-based sensor using wax printing, similar to Wang *et al.*[91] work, and the three-electrode system using a stencil technique, identical to Prasad *et al.*[92] The sequence of a complementary miRNA target was identified using differential pulse voltammetry (DPV) with a thiol-linked synthetic DNA probe placed onto the working electrode in a redox$[Fe(CN)_6]$ solution. Hybridization was recognized on the paper-based biosensor based on the difference in redox probe signal in the presence/absence of miRNA hybridization. Here hybridization efficiency is calculated using the equation and using voltammograms given in Fig. 6b and c

$$\mathrm{HE}\% = \frac{\frac{\Delta I}{100}}{I_{\mathrm{probe}}} \quad (1)$$

where $\Delta I = I_{\mathrm{hybrid}} - I_{\mathrm{probe}}$ and the highest HE % calculated was around 37.1% for miRNA-155 and miRNA-21 target hybridization. The LOD was around 0.19 μg mL^{-1} for miRNA-155, whereas it was around for miRNA-21. The sensitivity was reported around 295.3 and 351.1 μA mL μg^{-1} cm^{-2} for AuNP/RGO-modified paper electrode comparing AuNP/MoS_2 – modified paper electrode.[93] Using a continuous and straightforward coating process (Fig. 7a), graphene and poly(3,4-ethylene dioxythiophene):poly(styrenesulfonate) (PEDOT:PSS) modified paper-based EIS aptasensor were constructed by Yen *et al.* for carcinoembryonic antigen (CEA) detection. This glycoprotein CEA has a molecular mass of almost 180–200 kDa.[94,95] It acts as a tumor marker and is critical in cancer detection and treatment. The presence of high levels of this tumor marker has been linked to various cancers, including breast, colorectal, ovarian, pancreatic, lung, and gastric cancers. This low-cost aptasensor detects CEA in a linear range of 0.77–14 ng mL^{-1} in standard buffer solutions and human serum samples. In both samples, the LOD for CEA was 0.45 ng mL^{-1} and 1.06 ng mL^{-1}, respectively.[96]

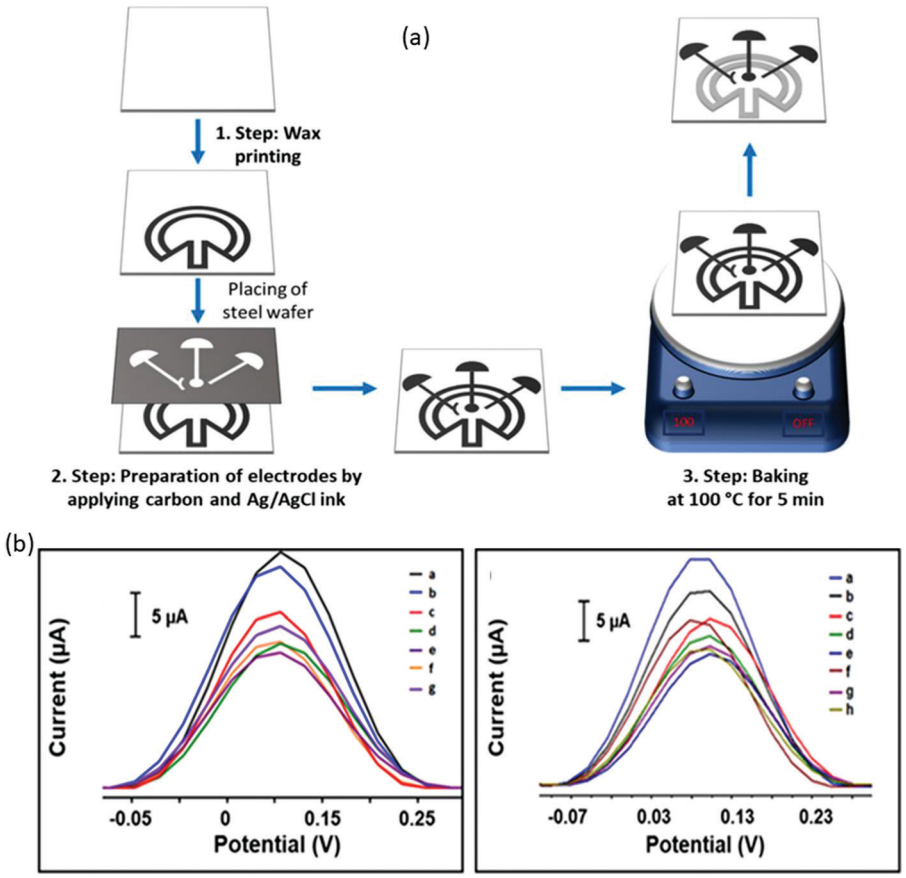

Fig. 6 (a) Steps involved in the fabrication of paper-based sensor for detection of microRNAs (b) Voltammogramms in the absence of microRNAs. Source: reprinted from H.Torul, E. Yarali, E. Eksin, A. Ganguly, J. Benson, U. Tamer, *et al.*, Paper-Based Electrochemical Biosensors for Voltammetric Detection of miRNA Biomarkers Using Reduced Graphene Oxide or MoS_2 Nanosheets Decorated with Gold Nanoparticle Electrodes, *Biosensors.*, 2021, **11**(7), 236.

Since pristine graphene lacks a semiconducting gap, it cannot be used in electronic devices. As a result, one of the most practical methods of controlling graphene's semiconducting properties is doping.[97] Boron-doped graphene is of particular interest because it can stimulate various chemical and electrochemical activities in the graphene basal plane.[98,99] Aside from boron-doped graphene, boron-doped diamond-graphene hybrid structures were another hotspot in carbon materials research. However, its use in immunosensors is limited. Hongji *et al.* realized this and created a boron-doped diamond (BDD)/vertical boron-doped graphene (BG) composite film coated with Au nanoparticle *via* CVD and electroplating, resulting in a high surface area and electrocatalytic activity. This immunosensor was capable of simultaneously quantifying carcinoma antigen 125 (CA 125) and CEA at concentrations of 0.5–100 pg mL^{-1} and 0.5–100 mU mL^{-1}, respectively, with LOD around 0.15 pg mL^{-1}. The simultaneous detection of CA125 and CEA was accomplished utilising a sandwich-type signal acquisition method that employed an electrochemical sensor based on BDD/Au-VBG as a working electrode, TB and Fc as redox probes, and Au–TiO_2 particles as a carrier.[100]

BRCA1 and BRCA2 are two specific breast cancer susceptibility genes discovered in human DNA. The BRCA (breast cancer abbreviation, typically pronounced bracka) genes are passed down from their parents to men and women. BRCA1 and BRCA2 are tumor suppressor genes that inhibit cancers from developing when they are activated. BRCA1 and BRCA2 mutations, on the other hand, are responsible for almost half of all hereditary breast cancer cases. As a result, the early detection of these genes is crucial. Breast cancer is currently diagnosed using mammography, PCR screening, ultrasound and other methods. However, due to its small size, this tumor is difficult to detect.[101,102] The surface plasmon resonance approach is now being utilized to collect data of DNA molecular bonding, allowing BRCA1 and BRCA2 breast tumors to be immediately detected to address the demand for effective and precise ways of breast cancer screening. Several methods are adopted to excite surface Plasmon, including coupling with fiber optics, prisms, nanoparticles, grating, *etc.* But increasing the sensitivity of this type of biosensor is a difficult task. In this regard, graphene is one of the materials explored extensively due to its excellent features. This substance has been shown to boost SPR sensitivity in various studies, both theoretically and empirically. The review work done by Nurrohman *et al.* discussed the latest development in graphene-based SPR biosensors.[103] Taking advantage of the most notable features of these graphene-based SPR biosensors, Hossain *et al.* described a very effective fiber-optic SPR biosensor for monitoring BRCA1 and

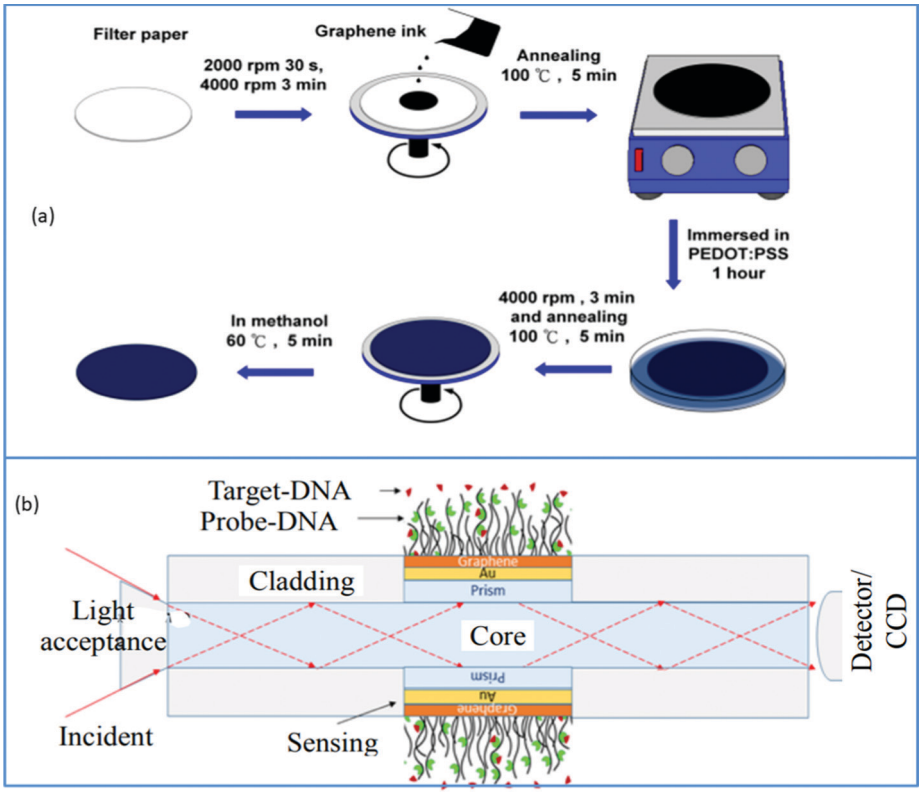

Fig. 7 (a) Steps involved in the fabrication and modification of electrochemical paper-based working electrode for the detection of CEA. Source: reprinted from Y.-K. Yen, C.-H. Chao, Y.-S. Yeh, A Graphene-PEDOT:PSS Modified Paper-Based Aptasensor for Electrochemical Impedance Spectroscopy Detection of Tumor Marker, *Sensors.*, 2020, **20**(5), 1372. (b) Schematic illustration of four-layered model for fiber optic SPR biosensor for detection of BRCA1 and BRCA2 breast cancer genes. Source: reprinted from Hossain MdB, Islam MdM, Abdulrazak L. F., Rana MdM, Akib TBA, M. Hassan, Graphene-Coated Optical Fiber SPR Biosensor for BRCA1 and BRCA2 Breast Cancer Biomarker Detection: a Numerical Design-Based Analysis, *Photonic Sens.*, 2020, **10**(1), 67–79.

BRCA2 breast cancer. They used an attenuated total reflection (ATR) approach to identify deoxyribonucleic acid (DNA) hybridization and individual point mutations in the BRCA1 and BRCA2 genes. Fig. 7b depicts the structural layout of this newly designed graphene-based fiber optic SPR biosensor. This suggested sensor may detect precisely matched and mismatched DNA interactions between probing and target DNA based on differences in the SPRF and SPR angle. This graphene-based SPR biosensor's improved sensitivity is owing to graphene's property to absorb light.[104]

Biological field-effect transistors (BioFETs) have yet to be recognized, despite their potential for substantially higher sensitivity and much faster quantification, with sensing devices primarily constrained to two-three electrodes electrochemical biosensors.[105,106] Graphene is employed as a sensing material in BioFETs because of its distinctive electrical and chemical characteristics. These graphene-based BioFETs exhibit a higher efficiency when run in an electrolyte gated approach without solid-state dielectric due to the electric double layer formed between the graphene and electrolyte.[107,108] This electrochemical gate is more effective than a typical SiO_2 back gate with a thickness of hundreds of nanometers.[109] Sotirios *et al.* reported an electrolyte gated PCB-based FET DNA for the first time. To enable label-free DNA sensing, graphene ink was drop-casted to produce the transistor channel, and PNA probes were placed on the graphene channel. After a fully inkjet-printing compatible construction approach, it was demonstrated that the sensor could specifically recognize the complementary DNA sequence. The first FET using a PCB was a core board as the substrate and PCB electrodes as the transistor source, drain, and gate pads. To maximize downsizing and integration, the traditional bulky reference electrode is substituted with an in-plane PCB electrode. This design hasn't gotten much attention in the literature. Fig. 8b given here shows that with reduction of gate voltage I_{ds} value decreases. This identifies the gate influence on I_{ds} and reveals the graphene's p-type behavior. The absence of apparent Schottky barriers at the graphene–electrode contact is indicated by the linearity of these curves. The LOD of this PCB-based FET was around 1 nm calculated using the curve shown in Fig. 8c, which is relatively high without microfluidic integration and biochemistry optimization. Furthermore, ssDNA detection is effective at this range of concentrations with excellent sensitivity (30.1 mV decade^{-1}). Their study demonstrate the inkjet printing's potential to incorporate semiconductor chips into Lab-on-PCB platforms seamlessly for the first time. This opens the way for inkjet-printed Lab-on-PCB platforms driven by printed, electronic circuits with significantly greater intricacy and processing capacity.[110] Niazul *et al.* suggested a biosensor utilizing a graphene field-effect transistor (GFET) functionalized with target-binding aptamers for detecting

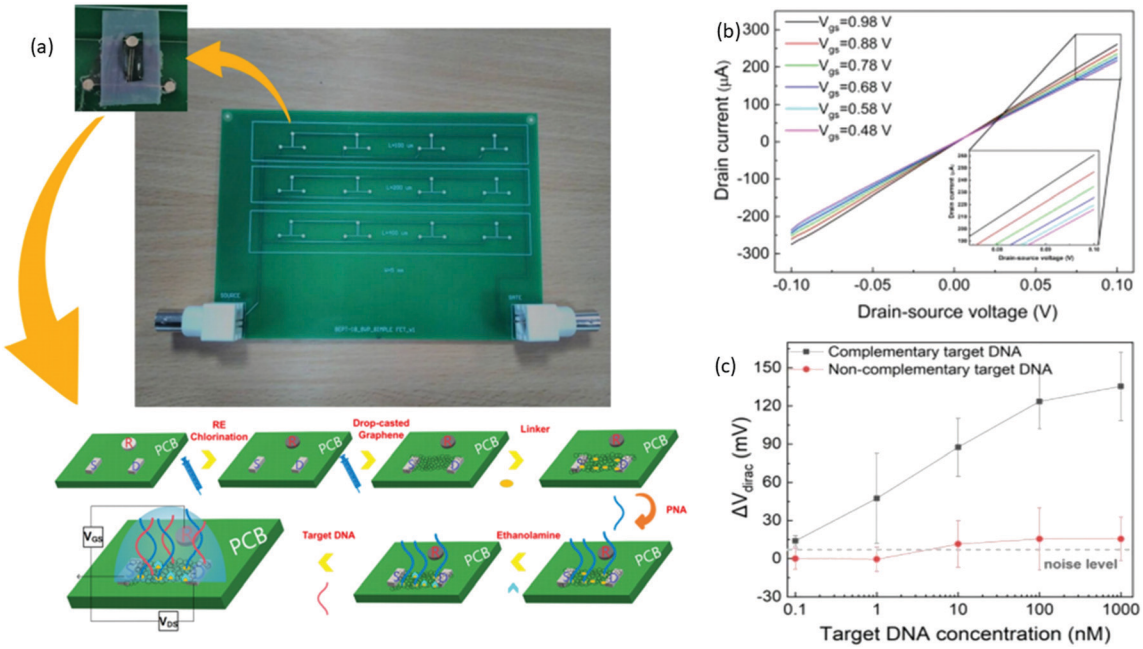

Fig. 8 (a) Printed circuit board-based graphene FET sensor (b) output curves of the graphene electrolyte-gated transistor (c) V_{Dirac} shifts for various complementary and non-complementary target DNA concentrations. Source: reprinted from S. Papamatthaiou, P. Estrela, D. Moschou, Printable graphene BioFETs for DNA quantification in Lab-on-PCB microsystems, *Sci, Rep.*, 2021, **11**(1), 9815.

the thrombin protein biomarker using a typical microfluidic fabrication approach. This sensor was used with microfluidic devices to produce good sensing performance. The previously published GFET-based microfluidic sensor, on the other hand, was not suitable for real-time applications since it lacked LOD in the picomolar range as well as a detection range in micromolecular concentration.[111]

The nanocomposite of rGO and Cys hydrogels could give an exciting substrate with large carboxylic groups leading to higher antibody loading, good stability, and strong surface absorption ability, leading to increased target molecule sensitivity.[112] Singh *et al.* developed a dual-modality microfluidic sensor for cardiac myoglobin sensing utilizing this Cys–rGO hydrogel. A patterned Au was first modified using rGO–Cys hydrogel before being inserted into a PDMS microchannel *via in situ* functionalization with specific cardiac myoglobin (cMb) antibodies utilizing EDC-NHS chemistry. Researchers used dual-modality performance employing differential pulse voltammetry and SPR methods to detect the cardiac myoglobin biomarker and perform the real-time binding kinetic study. They used an SPR technique in plasmonic detection mode to find out cMb concentration using antibodies-antigen interaction on the surface of the microfluidic sensor. The surface density of immobilized cMb molecules above the Cys-RGO hydrogel is determined using the equation

$$A = \frac{\Delta\text{Response}\,[m^0]}{\text{Conversion factor}\left[m^0.\left(\frac{\text{mm}^2}{\text{ng}}\right)\right]} \quad (2)$$

where A denotes the surface density of immobilized cMb. Eqn (2) is used to calculate the quantity of immobilized cMb using this surface density. Also, the number of cMAbs bound onto the hydrogel is determined using eqn (3)

$$\text{Amount} = \text{Surface density (ng mm}^{-2}) \times \text{surface area (mm}^{-2}) \quad (3)$$

$$N = \frac{\text{Amount (ng)}}{\text{Molar mass}\left(\frac{\text{g}}{\text{mol}}\right)} \times \frac{10^{-9}(\text{g})}{\text{ng}} \times 6.022 \times 10^{23}(\text{mol}^{-1}) \quad (4)$$

The number of cMAb molecules over the surface of this sensor was around 1.38×10^{15}. The SPR angle was also shown to rise with increasing concentration, which can be attributed to improved kinetic binding between this cMb and cMb conjugated hydrogels. Here DPV sensing of the conjugated hydrogel sensor shows LOD of 4 pg mL^{-1} with sensitivity around 196.66 μA ng mL^{-1} cm^{-2}. In contrast, the SPR sensing exhibited LOD 10 pg mL^{-1} with around 42.86 m ng^{-1} mL^{-1}.[113]

2.1.2 For biomolecule detection. *In vitro* analysis requires particular biomarkers for preliminary disease diagnosis. Small metabolic molecules such as glucose, dopamine and hydrogen peroxide (H_2O_2), which have specific concentrations suggesting definite pathogenic processes in biotic fluids, could be utilized as biomarkers to diagnose diseases early.[114–116]

2.1.2.1 For glucose detection. The Laser induced graphene (LIG) has been utilized either in its pure state or combined with other composite materials to create microfluidic prototypes to detect glucose.[117] LIG-based bioelectrodes were used to develop PDMS-based microfluidic biofuel cells by Prakash *et al.* This LIG derived from PI sheets was incorporated into a microfluidic device made of PDMS using traditional soft lithography. During the irradiation procedure, the CO_2 lasers' power and speed were

tuned. They submerged LIG in a linker solution with 1-ethyl-3-(3-dimethyl aminopropyl) carbodiimide to bind the glucose oxidase and lactase on the sensor surfaces. The enzyme solutions were drop-cast on the irradiated surface and left for 2 hours at RT for the immobilization process. PET sheets were sliced using a Y-shaped microchannel to create the microfluidic cells. A microchannel structure was built using PDMS template curing, where this microfluidic cell shows the fluid rate and power density of around 200 μL min^{-1} and 13 μW cm^{-2}. Here electrochemical redox reactions and polarisation processes in the microfluidic environment contributed to the developed system's exceptional performance. This sensors linear range was around 10–40 mm, and the current increased linearly as the voltage increased.[118] Bipolar electrode (BPE)-based electroluminescence (ECL) sensors have recently gained popularity and recognition due to their high specificity, simple instrumentation, good selectivity, lack of background signal and controllability. This device is very simple to operate with quick processing and multiplexing. Manish *et al.* fabricated a compact 3D printed ECL sensor with LIG-based open BPE. Graphene was synthesized utilizing CO_2 laser ablation over polyimide (PI) sheets. They injected H_2O_2 and luminol into the microchannels to detect H_2O_2, and when a sufficient voltage is given to the driving electrode, a redox process begins. As a result, on the anodic face of the BPE, an ECL signal is formed, which may be caught using a smartphone. The reaction of H_2O_2 with luminol is as follows

$$\text{Luminol} - e^- - H^+ \text{ Diazoquinone} \quad (5)$$

$$H_2O_2 + \text{Diazoquinone Luminolendoperoxide} \quad (6)$$

$$\text{Luminolendoperoxide } N_2 + \text{3-aminophthalate} \quad (7)$$

$$\text{3-Aminophthalate 3-aminophthalate} + h\gamma \quad (8)$$

The BPE anode was treated with GO_X and maintained at room temperature (RT) for around 5 minutes to detect glucose. Following that, an equal amount of luminol and glucose was injected into the channel. With optimizing parameters like pH, luminol concentration, applied voltage, channel length and so on, this sensor shows LOD around 0.138 μM and 5.8729 μM for glucose and H_2O_2, respectively.[119] He also built a LIG-BPE-ECL sensing platform using the same laser ablation process, but they made a closed BPE rather than an open BPE. Here Individual sensing of Vitamin C, vitamin B12, and H_2O_2 with linear ranges of 0.5–1000 nM, 1–1000 M and 0.5–100 M with LOD of 0.109 nM, 0.96 M and 0.303 M were used to verify the performance of this two-channel BPE-ECL-LIG-C device. Following that, a three-channel BPE-ECL-LIG-C device was created and concurrent detection of Vitamin C and Vitamin B12 was also achieved.[120] Instead of these two and three-channel electrode systems, they validated a LIG-based single electrode (SE) system for enzymless ECL detection of multiple analytes. Using this sensor, they carried out the detection of H_2O_2, glucose, dopamine and xanthine in the linear range from 0.1 to 70 μM, 0.1 to 70 μM, 0.1 to 100 μM and 0.1 to 100 μM with a LOD around 1.71, 3.76, 3.40 and 1.25 μM respectively.[121] Manish *et al.* developed an ECL device with a U-shaped bipolar electrode (U-BPE) for enzymless sensing of different biomarkers. With LODs around 2.51, 4.36, 4.01, and 5.32 μM, this ECL sensor was utilized to detect D-glucose, H_2O_2, choline, and lactate, among other biological analytes.[122]

Incorporating conductive materials such as graphite, GO and carbon nanotubes into chitosan-modified electrodes leveraging chitosan's biocompatibility was a potential strategy to enhance the selectivity and sensitivity of paper-based electrodes (μPAD). Using this strategy, Rokemono *et al.* created a chitosan/GO modified PAD for paracetamol and glucose electrochemical sensing by using simple solution casting and UV curing followed by coating with carbon paste. Here the impedance results show that the electron transfer process at the electrode/analyte solution contact accelerates with increasing analyte concentration. CV experiments show a linear response for analyte concentrations ranging from 2.5 to 100 M. Furthermore, regardless of the analyte, the sensitivity of the modified paper-based electrode rises with a different proportion of GO. By utilizing electrode coated with chitosan/GO (5 wt%) composites, the highest sensitivity for paracetamol sensing is 16 mA mM^{-1} and for glucose, sensing is around 4.4 mA mM^{-1}.[123] Cao *et al.* reported a paper-based microfluidic chips in point-of-care devices (POCD) employing 3D μPAD. Whitesides team's invention of 2D and 3D μPADs in which fluid motion occurs inside diverse microfluidic channel designs due to capillary driving force inspired them to create this electrochemical glucose biosensor. Here the aldehyde functionalized μPAD was manufactured using periodate oxidation. The new 3D μPAD type was made utilizing photolithography, whereas screen printing technically produced 3D paper-based electrodes. This electrochemical sensor's working electrode was made from a Prussian blue-deposited rGO-tetraethylenepentamine (PB/rGO-TEPA) composite. In contrast, the counter/working electrode was aldehyde functionalized and employed to immobilize GOD. This sensor exhibits LOD around 25 μM over a broad linear range of 0.1–25 mM. Because of the excellent wettability of this paper-based electrode, when glucose was dribbled into the hydrophilic detecting region, it immediately came in contact with the GOD immobilized in the hydrophilic area, causing a particular enzyme-substrate interaction to create H_2O_2, as illustrated in the reaction formulae (1) and (2). The produced H_2O_2 was disseminated over paper by capillary action and reached the surface of the PB/rGO-TEPA modified electrode almost quickly. The PB immobilized on the surface of electrode was reduced to Prussian white (PW) while the electrode was functioning. Because of PW's excellent electrocatalytic reduction activity, H_2O_2 may be reduced, and PW can be oxidized to regenerate PB, as illustrated in reaction formulae (11) and (12).

$$\text{GOD(FAD)} + \text{Glucose GOD } (FADH_2) + \text{Glucose acid} \quad (9)$$

$$\text{GOD } (FADH_2) + O_2 \text{ GOD(FAD)} + H_2O_2 \quad (10)$$

$$KFe^{3+}[Fe^{2+}(CN)_6](PB) + e^- + K^+ K_2Fe^{2+}[FE^{2+}(CN)_6](PW) \quad (11)$$

$$K_2Fe^{2+}\,[FE^{2+}\,(CN)_6](PW) + \tfrac{1}{2}\,H_2O_2\;KFe^{3+}[Fe^{2+}\,(CN)_6](PB) + OH^- + K^+ \quad (12)$$

The use of this rGO-TEPA/PB composite as electrode modification materials allows for electron transport between the GOD and the electrode and considerably amplifies the current signal and improves reaction sensitivity. As a result, the change in decrease peak current produced by a change in glucose concentration can be utilized to quantify glucose.[124] A graphene-based field-effect transistor (GFET) has been used as a sensor by immobilizing bioreceptors on its surface while offering a controlled environment for monitoring and detecting biological/physiological processes. When an electric field is applied to the graphene surface, charged molecules induce an electrical reaction in GEFT.[125] The GFET has been effectively used to fabricate a high-performance glucose monitor thanks to graphene's enhanced electrical conductivity and unique structure. However, the commercially available bulk G-FET devices are enzymatic, and enzyme deactivation commonly compromises the precision and durability of these devices. Furthermore, they are frequently made on solid substrates (such as glass or silicon), limiting their wearability. For non-enzymatic glucose sensing, a flexible ultrathin affinity-based G-FET was fabricated by Yao *et al.* This device was fabricated on an adhesive support, which allowed it to be easily peeled off and simplified the operation. The specific pyrene-1-boronic acid (PBA) was used to functionalize the graphene channel. When glucose molecules were injected into these graphene channels, electron-withdrawing PBA molecules recognized them. They formed glucose-boronate ester complexes, which are electron-rich, causing the conductivity of the graphene channel to change. This sensor shows a LOD of around 0.1 μM over a broad detection range of 1–0.5 mM.[126] Wiorek *et al.* fabricated an epidermal pad for glucose analysis in perspiration that incorporates temperature and pH correction based on local dynamic sweat change during on-body measurements. The calibration parameters are modified to any change in temperature or pH throughout the athletic exercise using a unique "correction technique," and this epidermal glucose biosensor (Fig. 9) has a linear response range within the physiological amounts of glucose in sweat (10–200 M). Furthermore, the sensor also has excellent reversibility, quick response time and good selectivity.[127]

2.1.2.2 For other small molecules detection. Fishlock *et al.* developed a modified electrochemical paper device (e-pads) for dopamine detection. The electrodes were positioned along the wax-defined microfluidic channel in this capillary flow device, using Whatman filter paper as the porous wicking substrate. The working electrode was implanted directly into Whatman filter paper using the paper as a precursor for LIG. This LIG is obtained by treating Whatman filter paper coated with flame-retardant spray, then treated with CO_2 infrared Laser. This treatment helps to produce a 3D porous graphene network with high electrical conductivity and high-surface–area. They prepared this counter and working electrode using Laser alongside the wax defined microfluidic channel where the reference electrode was prepared using inkjet-printed silver. The prepared

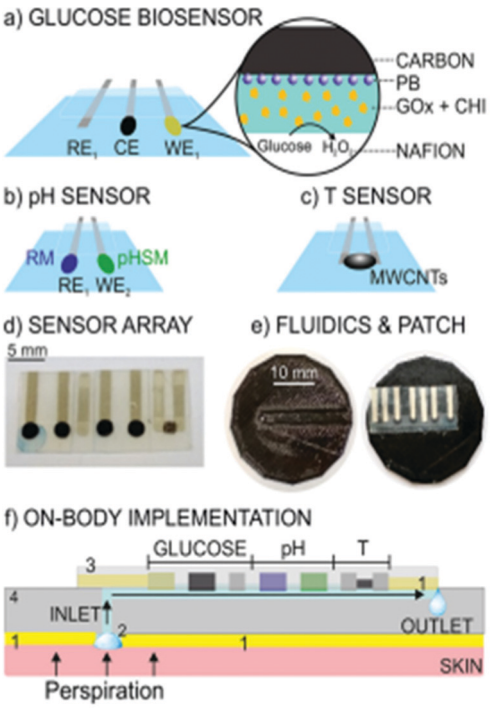

Fig. 9 (a) Glucose, (b) pH potentiometric and (c) temperature sensor (d and e) image of microfluidic sensor (f) illustration of microfluidic sensor attached to the skin. Source: reprinted from A. Wiorek, M. Parrilla, M. Cuartero, G. A. Crespo, Epidermal Patch with Glucose Biosensor: pH and Temperature Correction toward More Accurate Sweat Analysis during Sport Practice, *Anal Chem.*, 2020, **92**(14), 10153–10161.

working electrode based on pristine graphene was functionalized using nitrogen and modified this *N*-functionalized graphene using MnO_2. This microfluidic devices helps in detection of neurotransmitters.[128]

GEFT was fabricated by Schuk *et al.* to measure the concentration of L-lactic acids in various fluids. Lactate dehydrogenase enzyme was used to functionalize the active surface of graphene. This work proved graphene's ability to monitor L-lactic acid accumulation in human samples, implying that this material might be employed in more basic and low-cost equipment, such as flexible sensors for POC.[129]

Cystatin C (Cys C) is a 13 kDa protein made up of a single 120-amino-acid polypeptide chain.[130] This serum's abnormally high levels have recently been revealed to be a prognostic sign for various conditions, including neurological problems, cardiovascular disorders, and cancer.[131,132] Shalini and Uma Maheswari fabricated a Cys C detecting nano interface electrochemical immunosensor. A glassy carbon working electrode (GCE) was modified with nanocomposites of GO-chitosan (GO-Chit), which was then translated onto a paper-based microfluidic substrate. They fabricated this paper-based substrate using screen printing where carbon ink formulation was screen printed over a wax-coated paper following screen printing of Ag/AgCl paste. Compared with the modified GCE, this paper-based sensor shows a LOD of 2.6 pg μL^{-1} with a sensitivity of around 15.5 μA ng^{-1}.[133] Yang and his team with the concept of a laser-engraved (LEG)

wearable bio-sensor that could be mass-produced to detect tyrosine levels (TYR) and uric acid (UA). A chemical sensor (LEG–CS) over polyimide for measuring low-level TYR and UA, a physical sensor (LEG–PS) for temperature and respiration monitoring and a multi-inlet micro-fluidic module for dynamic sweat sampling are all included in this device. Electrochemical sensors use raster engraving, while microfluidic and biological sensors use vector engraving. This sensor had a sensitivity of 0.61 and 3.50 50 μA μM^{-1} cm^{-2} for Tyr and UA, respectively, with LOD of 0.74 and 3.6 μM. This sensor-relied on LEG exhibited excellent selectivity at physiologically acceptable levels compared to other sweat studies.[134] Stojanovic *et al.* fabricated a tiny microfluidic chip to detect ascorbic acid selectively. This microfluidic channel was created using the xurography procedure with a microfluidic channel between two silver electrodes. To enhance the conductivity and the electron transfer mechanism, a graphene sheet was placed between the gaps of these electrodes. The sensing mechanism for this microfluidic platform was based on an increase in overall conductivity as ascorbic acid concentration increased, resulting in an increase in capacitive parameters and a decrease in resistive parameters and an increase in the suggested equivalent electrical circuit[135]

2.1.3 For pathogen detection. Viral infections are among the leading causes of serious pandemics and infectious illnesses, resulting in billions of dollars in economic losses each year and thousands of deaths. In the instance of COVID-19, global economies were shut down for months, and physical separation, along with severe changes in the social behavior of many persons, resulted in a slew of problems for all countries. As a result, developing a speedy, low-cost, and sensitive viral detection method is crucial for improving human living standards while utilizing biomedicine, bioresearch and security also environmental science. Graphene has emerged as a viable material for microfluidic biosensor fabrication due to its several fascinating properties, including exceptional conductivity, ultra-high electron mobility, and remarkable thermal conductivity.[136] As a result, graphene-based analytical LOC and microfluidic devices have been proven to be capable of detecting a wide spectrum of viruses, from the decades-old Influenza virus to the more recent SARS-CoV-2 virus. Recently Sengupta *et al.*, for the very first time, reviewed graphene-based LOC devices to detect viruses. This review covers the widest variety of viruses detected by graphene-based LOC devices, including SARS-COV.[137] Because this section covers most of the current advancements in microfluidic devices for virus detection, we'd want to look into some recent studies that Sengupta *et al.* did not include. Recently, graphene-based microfluidic sensors were successfully used to detect SARS-CoV-2, prompting researchers to examine current advancements in graphene-based microfluidic platforms for Covid-19 detection. As a result, the major thrust after 2019 was in this area. A powerful urge exists to create a specific and sensitive assay for detecting antibodies to SARS-CoV-2 virus within minutes, if not seconds; preferably, within days of infection, which would be especially valuable in medically deprived areas if the reading could be done on a smartphone. For identifying infections or antibodies, electrochemical sensing is a potential approach. In this method, electrochemical transduction is employed to detect the formation of antibody–antigen complexes. Aside from assay and antigen protocols, the shape and surface chemistry of the electrodes employed in an electrochemical cell have an impact on specificity, sensitivity, and detection time. Ali *et al.* effectively created a 3D device geometries with high aspect ratio ratios for electrodes for covid-19 detection in compared to a 2D planar construction. This device is built by employing 3D-printing gold micropillar array electrodes with an Aerosol Jet nanoparticle, then functionalizing rGO nanoflakes and immobilizing antigens over the electrode surface with an NHS: EDC chemistry. Electrochemical transduction was used to detect antibodies in the fluid by creating an immunocomplex with antigens over the surface of the 3D electrode. Antibodies against the S1 virus spike and antigen RBD were found at analytical sensitivity levels of 1×10^{-12} and 1×10^{-15} m, respectively. This device is generic, and it can detect biomarkers for various infections such as Zika, Ebola and HIV.[138] Sindre *et al.* developed a label-free biosensor for sensitive, fast, label-free, and amplification-free detection of SARS-CoV-2 using graphene as a working electrode integrated onto a flex printed circuit board (FPCB). Here SARS-CoV-2 capture ssDNA sequence was coupled with biotin to create a biotinylated probe, which was then fixed on a graphene surface modified with streptavidin. The hybridization of target DNA was accomplished using the sensing matrix that was constructed. A user-friendly reservoir chamber module was also built to convey the sample solution to the FPCB device's working electrode. This sensor's effective design boosted its sensitivity and selectivity, allowing it to detect DNA at concentrations ranging from 100 fg mL^{-1} to 1 g mL^{-1}. With a small amount of material, the electrochemical method paired with FPCB allowed for quick identification of the target sequence (5–20 L). They were able to get a LOD of roughly 100 fg mL^{-1}.[139] Another label-free impedance biosensor utilizing the screen-printing method was reported by Ehsan *et al.* to detect SARS-CoV-2. They demonstrated a low-cost batch production process for a cellulose paper substrate. A highly conductive graphene/carbon ink mixture was screen-printed as a working electrode to immobilize with IgG antibodies in various formats. These formats include 1-pyrenebutanoic acid succinimidyl ester (PBASE) direct format and staphylococcal protein A (Prot A) controlled format shown in Fig. 10, which were both characterized using electrochemical techniques. Fig. 10 depicts the EIS responses of this sensor, where both formats show a rise in the R_{ct} semicircle in the Nyquist plot when the concentration of spike protein increases. However, in the case of Prot A format, the linear range was enlarged three times in magnitude of concentration, which can be attributed to the antibody's ordered orientation *via* Prot A modifications. The EIS sensors given here can measure concentrations as low as 0.25 fg mL^{-1}, allowing early identification and isolation of the sick person.[140]

Other recent articles on graphene-based microfluidic and LOC sensors for viral detection focus on Hepatitis B virus detection (HBV). Because of the high death rates linked with cirrhosis, chronic hepatitis and liver cancer, this is a chronic viral infection

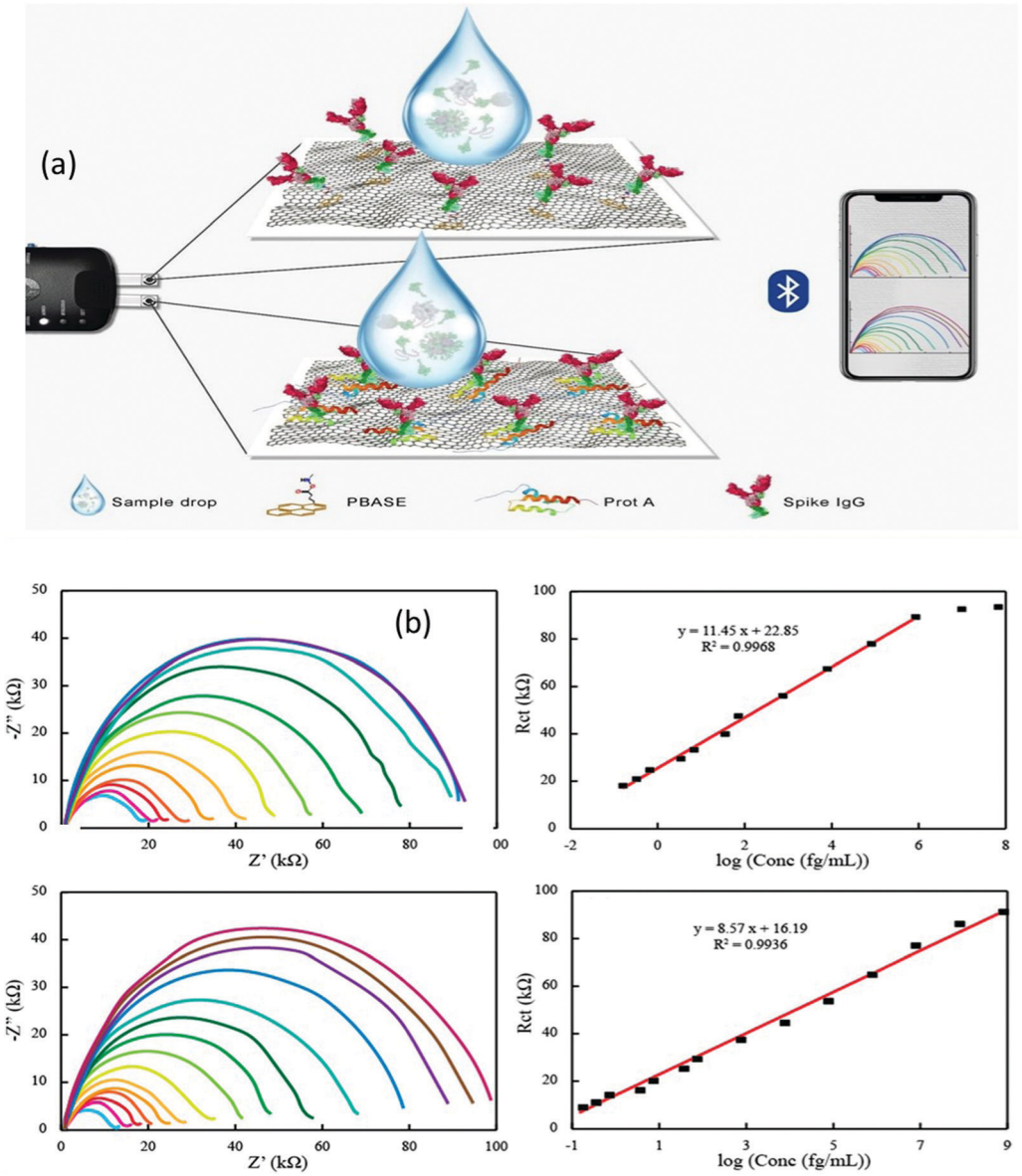

Fig. 10 (a) Schematic illustration of the fabricated sensor (b) sensor response and corresponding calibration plot using PBASE-mediated and ProtA-mediated antibody immobilized electrode on graphene. Source: reprinted from M. A. Ehsan, S. A. Khan, A. Rehman, Screen-Printed Graphene/Carbon Electrodes on Paper Substrates as Impedance Sensors for Detection of Coronavirus in Nasopharyngeal Fluid Samples, *Diagnostics*., 2021, **11**(6), 1030.

that is a serious worldwide health problem. Teengam *et al.* created a portable immunosensing sensor based on a smartphone that was successful in detecting HBV. The level of HBsAg was measured *via* amperometric detection and wireless communication *via* a card-sized NFC potentiostat. The HBsAg level was quantified by amperometric detection using a card-sized NFC potentiostat as wireless communication. This sensor's working electrode was built of screen-printed graphene (SPGE) that has been modified with gold (Au) nanoparticles to improve sensitivity, and β-cyclodextrin (β-CD) was electropolymerized on the surface of Au coated SPGE to trap antibodies. The LOD and linear calibration curve for HBsAg were determined to be 0.17 μg mL^{-1} and 10–200 μg mL^{-1}.[141] They were utilizing the advantages of Electrochemical paper-based devices (ePADs). Boonkaew *et al.* fabricated an ePAD for sequential immunosensing fluid administration by combining dual flow characteristics (delayed/fast) into a single paper device for simultaneous determination of hepatitis C core antigen (HCVcAg) and hepatitis B surface antigen (HBsAg). The redox reagent was stored in a delayed channel for future electrochemical experiments, while unbound antigens were washed automatically in a fast-flow channel. As a result, the user is unlikely to need the inconvenient multi-step reagent manipulation technique. The suggested ePAD had a LOD of 1.19 pg mL^{-1} for HCVcAg and 18.2 pg mL^{-1} for HBsAg.[142]

2.2 For chemical analysis

Pumera and his colleagues employed graphene-based nanoparticles in LOC devices for electrochemical detection.[143]

However, they could not identify any advantages to using GO as an electrochemical sensor in a microfluidics system at the outset.[144] Later, they realized that graphene that had been electrochemically reduced could be utilized as a sensor with excellent results. They also suggested that utilizing a graphene-based electrochemical sensor could increase the detection limits of other nanomaterials (such as silver nanoparticles).[145] Pungjunun *et al.* created an electrochemical paper-based device to detect lead Pb(II) and tin Sn(II) in canned foods. They made a sensor based on bismuth nanoparticles (BiNPs)/screen-printed graphene electrodes because nanocomposite containing metal nanoparticles and graphene improves the performances of electrochemical sensors synergistically. Because their oxidation potentials are near to each other, simultaneous detection of Pb(II) and Sn(II) results in an overlapping peak. They were able to improve the peak separation between these peaks as well as the signal by adding the surfactant cetyltrimethylammonium bromide (CTAB). Under ideal conditions, both metals have a linear range of 10–250 ng mL^{-1}, and the computed LOD (3SD/slope) for Pb(II) and Sn(II) was 0.44 ng mL^{-1} and 0.26 ng mL^{-1}, correspondingly.[146] On-chip optical gas sensors that use resonance shifts of cavities to measure molecule concentrations provide high sensitivity, real-time detection, and a tiny footprint. However, such sensors are typically hampered by a considerable cross-sensitivity problem induced by environmental temperature variations. To overcome this limitation, Wang *et al.* studied a dual-mode graphene-on-microring resonator that could precisely quantify gas concentrations while being unaffected by temperature fluctuations. To be more explicit, the modal linear independent responses may be employed to decouple the effects of external temperature variations and gas-induced graphene optical conductivity changes on the effective refractive indices of TE0 and TE1 modes in the resonator. Using this technology, they developed a nitrogen dioxide (NO_2) sensor with LOD around 0.5 ppm and sensitivity around 0.02 nm ppm^{-1}. Their research lays the path for developing high-sensitivity, temperature-stable on-chip optical gas sensors.[147]

3. MXene-based microfluidic sensors

MXenes and their hybrids have shown a great deal of promise in the realm of flexible, portable electronics, such as wearable sensors and microfluidic chips. Because of its flexibility and robust laminar structure, MXene could be easily integrated into microfluidic chips and wearable sensors.[148] Sensing electrodes are crucial in the creation of wearable sensors that use the electrochemical technique. In wearing technology, traditional metal-based electrodes have been replaced by innovative 2D materials like MXene to increase sensor performance by expanding contact area and adding appropriate electrical and mechanical qualities.[149]

3.1 MXene-based microfluidic biosensors

3.1.1 For biomolecules detection. Electrochemical biosensors built using the MXene-incorporated microfluidic chip are relatively new, yet they are quickly gaining popularity. Li *et al.* used an alternate approach, a cellulose-paper-based substrate, to create a highly integrated sensing (HIS) paper to detect lactate and glucose in sweat. They made this sensor utilizing a screen-printing approach using MXene/Methylene blue as the active material and foldable cellulose substrates as sweat analysis pads. This sensor's 3D layout optimizes sweat absorption by limiting fluid gathering and thereby lowering user discomfort. The fabricated device was made up of a sweat adsorbing vortex-patterned layer (the layer in touch with the skin), a 3D electrode layer, and a fast diffusion layer where the independent 3D position of three-electrode helps in gaining stability. After folding the aforementioned HIS paper-based substrate into a multi-layer structure, a well-designed 3D diffusion channel was created by linking hydrophilic regions of each layer. MXene-incorporated paper-based sensors are pretty unfamiliar and rapidly emerging. This is the first time such a revolutionary dual-channel system has been reported. With a sensitivity of 0.49 μA mM^{-1} and 2.4 nA μM^{-1}, this HIS electrochemical sensor can detect lactate and glucose at the same time. MXene acts as a highly sensitive interface, in this case, allowing the biomolecule to be immobilized. In contrast, its modification with MB allows for charge migration and improves the sensor's sensitivity.[150]

Zhang *et al.* reported a portable electrochemical patch sensor for real-time monitoring of potassium [K^+] ion concentration in human sweat. They used a layer-by-layer deposition method over PET substrate to fabricate this unique all-solid-state [K^+] ion-selective electrode based on MXene/MWCNT hybrid structure. For real-time detection of [K^+] ions, this flexible patch sensor was coupled into a battery-free RF energy harvesting Near Field Communication (NFC) wireless patch system. In this electrochemical patch sensor, a microfluidic channel was constructed utilizing 3D printing technology to collect human sweat and reduce sensor surface contamination. This sensor showed a sensitivity of roughly 63 mV dec^{-1}, which may be amplified to 173 mV dec^{-1} utilizing NFC, with a linearity of 1 to 32 mM.[151]

Another electrochemical microfluidic device for the analysis of creatinine, uric acid, and urea in whole blood was disclosed by Liu *et al.*, which can be used to assess bodily conditions during hemodialysis shown in Fig. 11a. This four-layered microfluidic device was created for continuous and direct multicomponent analysis of whole blood. A blood flow channel was on the top layer, a dialysis membrane was on the second layer, an isotonic solution channel was on the third layer, and a detecting chamber with a sensing electrode was on the bottom layer (screen printed MXene). To enhance the efficiency of this microfluidic electrochemical sensor, methylene blue (MB) was loaded onto this screen-printed electrode following immobilization with urease with the help of glutaraldehyde for urea measurement. The simultaneous detection of many analytes was achieved thanks to the synergistic effects of MXene electrocatalysis, enzymes immobilized on MXene and probes/ions adsorbed by MXene nano-sheets. The microfluidic chip was carefully designed to suit the requirements of complete blood

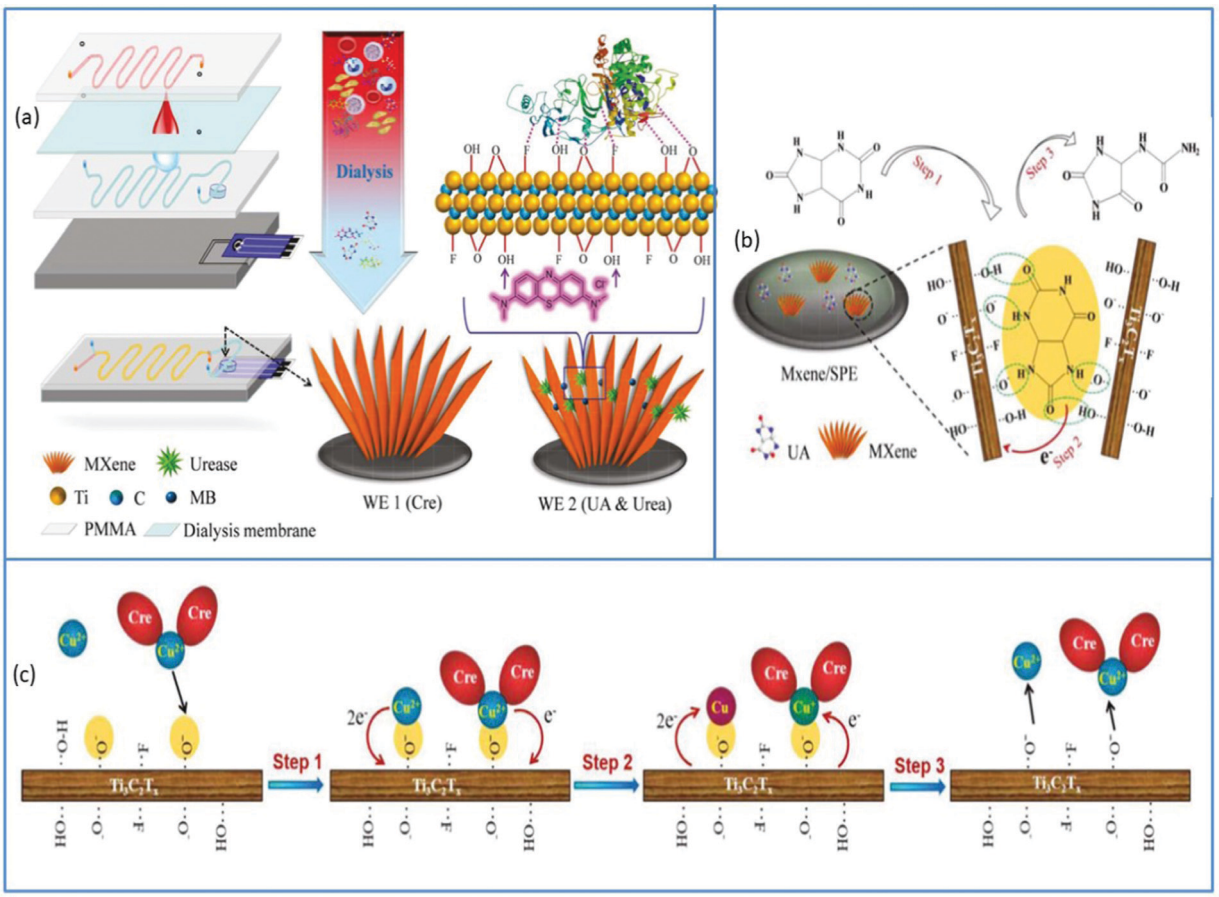

Fig. 11 (a) Schematic illustration of the fabrication of MXene based microfluidic sensor (b) UA detection mechanism and (c) creatinine detection mechanism. Reprinted with J. Liu, X. Jiang, R. Zhang, Y. Zhang, L. Wu, W. Lu, *et al.*, MXene-Enabled Electrochemical Microfluidic Biosensor: Applications toward Multicomponent Continuous Monitoring in Whole Blood, *Adv. Funct. Mater.*, 2019, **29**(6), 1807326. with permission from John Wiley and Sons.

analysis while also allowing for easy electrode replacement for long-term application. This chip was utilized to test the renal function in 105 healthy persons, with a gold standard being a conventional biochemical analysis apparatus. The content of Cre, urea and UA obtained by the chip method matched that obtained by the golden approach, and there was no statistical difference between the two procedures. The electrocatalytic mechanism of UA in the sensor is depicted in Fig. 11b. MXene adsorbs UA molecules, which form hydrogen bonds with the functional groups of MXene, increasing the effective concentration of UA at the electrode/electrolyte interface for subsequent electrocatalysis. In the instance of Cr shown in Fig. 11c, the Cre molecules will be entirely chelated with Cu ions, especially in the presence of excess copper (Cu) ions, and adsorption on MXene will be mediated by electrostatic interactions.[17]

3.2 For chemical analysis

Because of its inherent high hydrophilicity, chemical composition, and robust electrochemical nature, MXene-based sensors are a viable option for pollution detection.[152] The potential applicability of MXene-based sensors for environmental applications has been described in a vast number of reviews. MXene based Microfluidic sensors for environmental applications, on the other hand, are still in their infancy. Yang *et al.* revealed the first on-chip SERS sensor for gas detection. The use of SERS in conjunction with microfluidic technology aids in detecting a tiny trace of gases. The microfluidic channel can consistently control small gas flow, which helps to overcome the reproducibility concerns plaguing SERS. Extra adsorption materials with high surface areas are the most popular technique for improving the efficiency of a gas sensor. However, when it comes to microfluidic sensors, such materials restrict the analyte away from the SERS hotspot while simultaneously interfering with the microflow. As a solution, they created a honeycomb-like 3D substrate using layer-by-layer colloidal self-assembly, which was then translated into a microfluidic chip using a process they devised. By permitting *in situ* vortices in the SERS hot zone to raise detection sensitivity by increasing molecule residence time. Following this, an ultra-flexible MXene adhered onto this 3D substrate that serves as a universal adsorption layer for various VOCs (*i.e.*, explosives-related indole, odoriferous benzaldehyde and 2,4-dinitrotoluene (DNT)). Compared to typical lithography-fabricated plasmon-based sensors, this transfer method helps to minimize manufacturing costs, which is desirable for practical application. They employed a standard least-square analysis (CLS) approach to split the SERS

spectrum and identify the actual concentration of each constituent utilizing chromatic barcodes to determine the accurate concentration of these VOCs. This microfluidic sensor exhibited LOD of around 10 and 50 ppb for DNT and indole.[153]

4. TMD-based microfluidic sensors

Many nanomaterial-based detectors have been incorporated into microfluidic systems to improve sensing efficiency, sensitivity, and detection limits.[154] TMDs with unique electrochemical properties, on the other hand, is gaining popularity due to their atomically thin layered 2D architectures, which allow for easy device fabrication and patterning. Graphene and graphene derivative nanomaterials have been studied extensively to offer ultra-sensitive detection in microfluidic devices, especially lab-on-chip systems.[155] TMDs also have 2D layered structure compared to graphene with appealing features such as capacitive solid behavior, superior conductivity, and a high surface-to-volume ratio, making them promising candidates for increasing microfluidic device performance.[155]

4.1 TMD-based microfluidic biosensors

4.1.1 For biomolecules detection. Recently, in fluorometric biosensors, many of the nanomaterials have been reported as nanoquenchers due to their high quenching efficiencies, high surface area and good biocompatibilities, such as graphene oxide,[156] gold nanoparticles[157] and carbon nanotubes.[158] Very recently, MoS_2 nanosheets were reported as efficient dye quenchers because of their ability to spontaneously absorb single-stranded DNA (ssDNA) using van der Waals force between the nucleobases and basal plane MoS_2, displaying high fluorescence quenching ability, which was used for small molecules and DNA detection.[159] The quenching ability of MoS_2 is unstable and would be impacted by oxygen and moisture present in the atmosphere.[160] Besides, like graphene, the electrochemically active sites can be significantly reduced due to its aggregation tendency in practical applications.[161] It is critical to conduct studies as soon as possible after synthesizing MoS_2 solution, which isn't appropriate for a typical DNA test.[162] However, the combination of other materials with MoS_2 may circumvent this constraint. A novel microfluidic biosensor based on MoS_2/MWCNT nanocomposite with 3D architecture was fabricated by yang *et al.* for the detection of DNA molecules. When compared to MoS_2, the generated MoS_2/MWCNT aqueous solution combined with microfluidics shown high quenching stability for over 75 days, which is acceptable for a regular DNA test. The microfluidic channels greatly reduce the sample volume and so ~fmol DNA detection can be displayed with a detectable fluorescence color in a matter of minutes using the microfluidic assay. The constructed sensor had a linear range of 0–50 nM and could detect 1 nM DNA. It enables high-throughput DNA analysis in a simple and quick manner. The large scale sensing studies of DNA could be possible by using the strong quenching stability of MoS_2/MWCNT aqueous system connected with microfluidics, which reduced the time for sensing studies and thereby describing that MoS_2/MWCNT can be a favorable nanocomposite for fluorimetric sensing.[162]

A little amount of research has been conducted to investigate the use of TMDs in increasing the performance of analytical LOC microfluidic devices. Considering these facts, Toh *et al.* presented simple, cost-effective and sensitive fabrication of LOC electrochemical microfluidic devices for H_2O_2 detection. They integrated group 6 2D layered TMDs (MoS_2, WS_2, $MoSe_2$ and WSe_2) prepared by *t*-BuLi exfoliation as detector surfaces inside the LOC devices *via* drop-casting method and evaluated their response for heme-based H_2O_2 biosensor. The high activity of the 1T phase is related to the high density of active catalytic sites on both edges and basal plane, high conductivity, capacitive behavior and high electrical conductivity, making them excellent for sensing applications. The exfoliation with *t*-BuLi generates single to few-layered TMDs containing metallic 1T phase. Fig. 12a depicts the chronoamperometric reactions of this 1T-phase WS_2 to varied H_2O_2 concentrations. The reduction currents observed with the 1T-phase WS_2-based LOC device outperformed the other 2D TMD materials. They demonstrated superior electrocatalytic activity, a LOD of 2.0 nM, a wide range of linear responses (20 μM to 20 nM and 2 mM to 100 nM), and good selectivity for real-time analysis.[155]

4.1.2 For pathogen detection. Salmonella is a food-borne pathogen, the causative agent of paratyphoid A fever and poses a severe threat to human health.[163] Several techniques, including molecular and immunological, for detecting Salmonella, but these methods face limitations such as expensive reagents and cross-reactivity.[164] The electrochemical process could overcome all the rules associated with traditional methods. Besides, in this method, a biological recognition element was also used to directly bind with Salmonella and change the electrochemical signal.[165] 2D materials have recently piqued researchers' interest because of their stability, electron transfer kinetics, and large surface area.[166] Because of its large surface area, MoS_2 has sparked a lot of attention, although it has low conductivity.[167] Compared to graphene with a too tiny bandgap, the bandgap in 2D MoS_2 enables a multifold increase in device sensitivity.[168] The proper tuning of the bandgap in 2D MoS_2 is possible *via* several methods, whereas in graphene, the modulation of the electronic band structure is complex.[169] Furthermore, when 2D MoS_2 is changed into tetragonal symmetry, its inherent electronic energy state changes from semiconducting towards conducting, making it appropriate for bioanalyte detection using electrochemical techniques.[170] Furthermore, compared to other 2D materials such as graphene, which do not give excellent electrical and chemical properties, 2D MoS_2 is compatible with the typical electrochemical system.[171] Because the 2D electron–electron correlations between Mo atoms promote the planar electron transfer behavior, MoS_2 with layered structures has distinct catalytic and electrochemical properties in perpendicular and plane directions, resulting in differences in electrochemical behaviors the edge and basal planes.[172,173] Singh *et al.* have designed positively charged MoS_2 nanosheets functionalized with cetyltrimethyl ammonium bromide for protein conjugation over microfluidics electrode to detect Salmonella typhimurium.

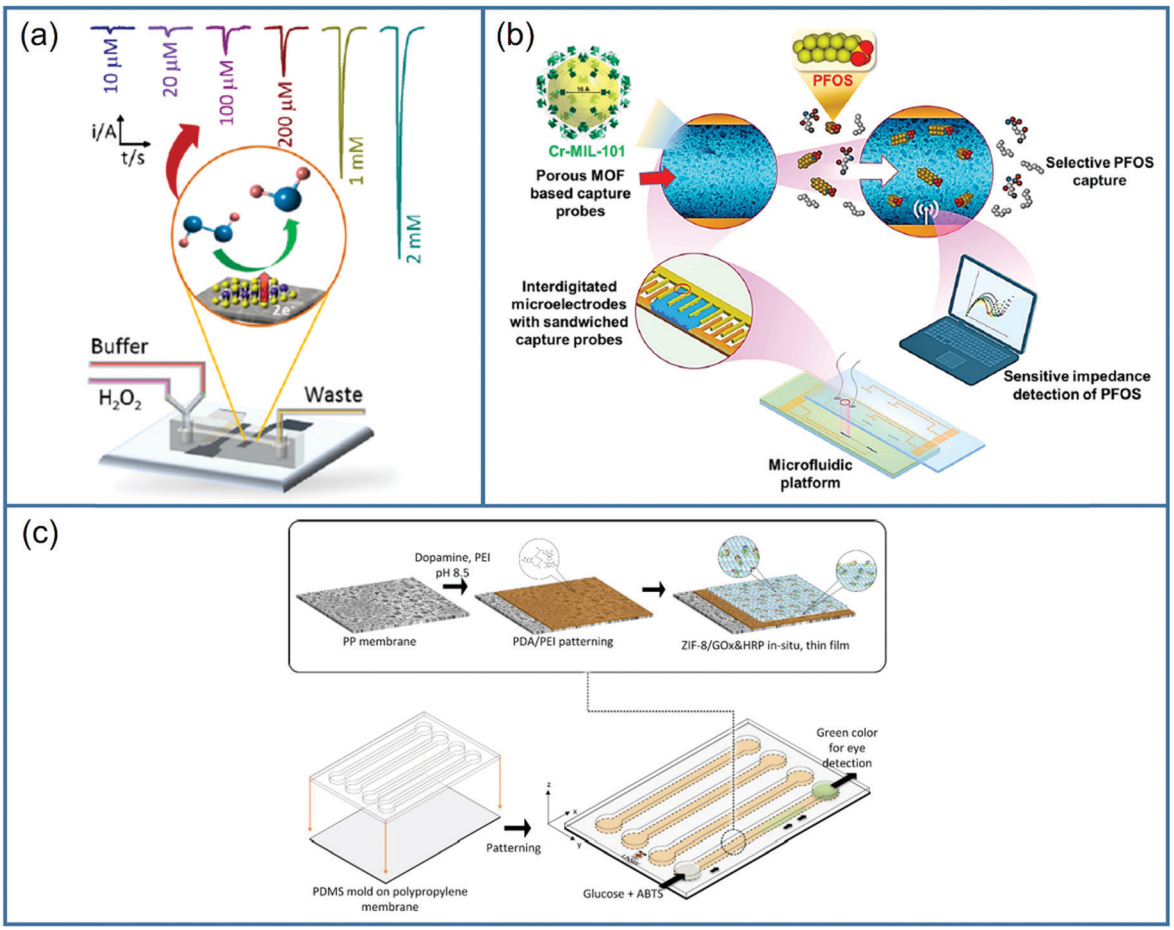

Fig. 12 (a) LOC based on TMD material for detection of H_2O_2. Reprinted with R. J. Toh, C. C. Mayorga-Martinez, J. Han, Z. Sofer, M. Pumera, Group 6 Layered Transition-Metal Dichalcogenides in Lab-on-a-Chip Devices: 1T-Phase WS_2 for Microfluidics Non-Enzymatic Detection of Hydrogen Peroxide, *Anal Chem.*, 2017, **89**(9), 4978–4985. (2020) American chemical society. (b) Schematic of perfluorooctanesulfonate (PFOS) detection using MOF based microfluidic sensors reprinted with Y. H. Cheng, D. Barpaga, J. A. Soltis, V. Shutthanandan, R. Kargupta, K. S. Han, *et al.*, Metal–Organic Framework-Based Microfluidic Impedance Sensor Platform for Ultrasensitive Detection of Perfluorooctanesulfonate, *ACS Appl. Mater. Interfaces.*, 2020, **12**(9), 10503–10514. Permission from (2020) American chemical society. (c) Fabrication of bio-composite containing MOF patterning reprinted with W. Qi, L. Zheng, S. Wang, F. Huang, Y. Liu, H. Jiang, *et al.*, A microfluidic biosensor for rapid and automatic detection of Salmonella using metal–organic framework and Raspberry Pi, *Biosens. Bioelectron.*, 2021, **178**, 113020. Permission from (2020) American chemical society.

Because CTAB provides a positive charge on MoS_2 sheets that forbid aggregation by countering the cohesive energy amid exfoliated layers, surfactant-assisted exfoliation for the production of MoS_2 could enable stabilization of exfoliated 2D MoS_2. CTAB-MoS_2 NS deposited the patterned indium titanium dioxide ITO microelectrode using the firm electrostatic contact of positively charged CTAB-MoS_2 NS. After this, a Lab on a Chip platform was developed by incorporating microelectrode with the PDMS microfluidic device for *S. typhimurium* detection *via* electrochemical impedance technique. The developed microfluidic immunosensor displayed excellent sensing parameters such as sensitivity 1.79 kΩ CFU^{-1} mL^{-1} cm^{-2}, the wide linear range of 10^1 to 10^7 CFU mL^{-1} and LOD of 1.56 CFU mL^{-1}.[174]

5. MOF-based microfluidic sensors

MOF-based biosensors have several advantages, such as porous structures, high catalytic activities, large specific areas, and ease of functionalization for developing highly efficient sensors. Despite the recent progress in preparing and applying different types of MOFs, the environmentally friendly synthesis by controlling their sizes and shapes remains a challenge. Furthermore, the lack of ease in operation, portability, integration and rapid assays in synthesized MOF biosensors limits their broad applicability in environmental analysis, biosensing, and POC detection, particularly in low resource situations. This versatile platform allows for rapid analysis, integrated processing, high portability and analysis of complex biological fluids with high sensitivity, efficiency and multiplexed detection. Among these advantages, microfluidics offers a unique chance for MOFs in controlled synthesis and sensing applications.[175,176]

5.1 MOF-based microfluidic bisensors

5.1.1 For biomolecules detection. Impressively, most of the MOF limitations are the advantages of microfluidic systems.

The integration of MOF-based biosensors on a microfluidic device can accompany each component providing huge potential for joined high-performance molecular detection in different areas. Researchers in past years have ventured to combine MOFs on microfluidics to develop biosensors benefiting from both MOFs and microfluidics. MOFs can be placed within microfluidic channels due to high pore volume, surface area and large functional groups; the MOFs-based microfluidic sensor can display high analytical performance. Increasing enzyme stability without affecting their activity is possible through biomineralization of enzyme in metal–organic-frame work (enzyme-MOF) composite, which has demonstrated great promise in biosensing devices.[176] Mohammed *et al.* fabricated a microfluidic biosensor based on MOFs and enzymes for glucose detection. However, many enzyme-MOF composites have focused on encapsulating enzyme particles, limiting synthesis flexibility for real-world applications due to the requirement for post-synthesis immobilization over solid support. Hence, the surface patterning and microfluidic system integration offer various advantages for developing a diagnostic sensing device based on the biomineralized enzyme. Polydopamine/polyethyleneimine coating was explored to pattern MOFs/enzymes in microfluidic channels for biosensors assembly in a PDMS-based microfluidic device. Fig. 12c depicts a schematic diagram of the production of bio-composite patterning. They used a cascade reaction of glucose oxidase and HRP enzymes on imidazole zeolitic framework-8 thin film to detect glucose. The ZIF-8/GO_x&HRP *in situ* displayed excellent selectivity and limit of detection at 8 μM with a wide concentration range from 8 μM to 5 mM for glucose detection. Initially, microfluidic devices were developed from PDMS or glass were followed by other polymeric materials such as PVA (poly vinyl alcohol), PMMA (polymethyl methacrylate), polystyrene, thereby widening the scope of microfluidic systems.[176] Since 2007, microfluidic paper-based sensors have emerged as a potential platform for several applications, including resource-limited settings and POC diagnostics.[177–179] Paper as a microfluidic platform offers various benefits over previously employed MEMS-based nanomaterials because of its ability to absorb aqueous fluids without active pumping, lightweight, thin, transport, easy to store, stack and compatible with biological samples and low cost. In 2019 Ilacas *et al.* developed MOF (encapsulate GO_x) based colorimetric sensor on two microfluidic paper platforms, one lateral flow assay based and the other based on the well configuration for glucose detection, followed Michaelis Menten enzyme kinetics. Furthermore, the LOD differs between platforms; experiments with the LFA-based platform showed sensitivity after 0.5 mM glucose, whereas the well-based μPAD was 0.25 $mmoL^{-1}$. This well-based μPAD platform is constructed of laminate sheets and multiple layers of wax-printed chromatography paper. The GO_x@MOFs species placed between the paper layers reacted with the glucose and KI solutions flowing through the device, producing a yellow-brown color. This device was dried, scanned, and examined, and a relationship between glucose concentrations and average inverse yellow intensity was discovered.[180] The devices created using MOFs as biomimetic catalysts should broaden the scope of microfluidic technologies for multiplex analyte detection.

5.1.2 For pathogen detection. The prevention of food poisoning is possible through the rapid screening of contaminated food. But the time-consuming cell culture prevents on-site detection using currently available bacterial detection methods; Eliza lacks sensitivity and PCR requires complex DNA extraction. Qi *et al.* fabricated a microfluidic biosensor based on raspberry pi and metal–organic framework NH_2-MIL-101 (Fe) with biological signal amplification *via* mimic peroxidase activity with a self-developed app to evaluate the color image data for the rapid, automatic and sensitive detection of salmonella. These MNB–Salmonella–MOF complexes were prepared using the simultaneous conjugation of target cells with anti-salmonella polyclonal antibodies modified MOFs and anti-salmonella monoclonal antibodies, which were further modified using immune magnetic nanobeads (MNBs) in a microfluidic chip. The complex catalyzed the mixture of H_2O_2 and OPD (*o*-phenylenediamine) to form yellow DAP (2,3-diaminophenazine). Finally, the bacterial concentration was calculated from the catalyst (DAP) analysis gathered under narrow-band blue light using a raspberry app. The outcome displayed outstanding ability to detect salmonella with a LOD of 14 CFU mL^{-1} and concentration ranging from 1.5×10^1 to 1.5×10^7 CFU mL^{-1}.[181] This microfluidic biosensor was capable of mixing, labeling, separating and detection. It demonstrated the advantages of using fewer reagents, being small in size, having a quick reaction time, and operating automatically to detect foodborne bacteria on-site.

5.2 For chemical analysis

The demand for sensing techniques that simultaneously provide high selectivity and sensitivity has increased because of public exposure to environmental, biological and chemical contamination from anthropogenic or natural sources and intentional chem-bio threats.[182] Developing techniques for highly selective, ultra-sensitive, and rapid *in situ* identification and quantitation of target contaminants could open up new technical and fundamental possibilities in biological/chemical/environmental/radiological forensics, as well as earlier disease detection and diagnostics and POCT applications. It facilitated the development of affinity-based analytical sensors with two crucial processes in target detection: (1) selective and preferential recognition of target from a sample matrix *via* particular affinity-based interactions; (2) the conversion of a target binding process into a measurable spectroscopic, magnetic or electrochemical response in a transduction step.[183] In light of these findings, a microfluidic impedance sensor based on MOF was developed for *in situ* detection of perfluorooctanesulfonate (PFOS). PFOS is a severe environmental pollutant that belongs to the per and polyfluoroalkyl substrates class of anthropogenic compounds. Their widespread civilian and industrial use has dramatically increased their earth's abundance. Schematics of PFOS detection are shown in Fig. 12b. This study used a synergic technique for affinity-based target capture using a porous sorbent probe placed on a microfluidic platform to boost detection sensitivity. A probe made of MOF Cr-MIL-101

with high pore volume and surface area was used for detection of PFOS based on the chromium center affinity toward both sulfonate functionalities as well as fluorine tail groups. This MOF based sensor integrated with microfluidic platform displayed ultrahigh sensitivity for the *in situ* detection of PFOS, the LOD was observed as 0.5 ng L^{-1}, which is similar to that of advanced *ex situ* techniques.[184]

6. Other 2D materials-based microfluidic sensors

The thermodynamically most stable form among the phosphorus allotropes is known to be phosphorene or black phosphorus. It is one of the potential candidates for biomedical applications because of its biocompatibility. Degradation is the major obstacle in using phosphorene in spite of its attractive advantages. The lone pair of electrons present in phosphorene reacts with O_2 to form an oxide that readily reacts with water to form phosphoric acid, this leads to Phosphorene degradation.[185] Marine algal blooms often grow during the summer months. Among these phytoplankton comes under harmful algal blooms (HABs) generate chemically stable compounds which adversely affect human health. Okadaic acid is a group of biotoxins that originate as a byproduct of HAB. It is a polyether fatty acid derivative and has been described as a major toxic compound in Diarrheic Shellfish Poisoning (DSP). In accordance with European standards, the maximum threshold level for OA in seafood is limited to 160 μg kg^{-1}. This low permissible level has prompted researchers to find out effective detection techniques. Ramalingam *et al.* have developed an electrochemical microfluidic biochip for the monitoring of OA. The aptamer-specific OA was immobilized on the screen-printed carbon electrode modified with phosphorene-gold nanocomposite synthesized without a reducing agent *via* an *in situ* one-step method. The signal strength was quantified using a redox pair of potassium ferro–ferri cyanide. The fabricated microfluidic platform improved the sensitivity, portability, and reaction time. The developed device consisted of specific channels for sample mixing and incubation. Altogether, the integrated system comprised of a PDMS microfluidic chip covering an aptamer modified SPCE, as a single detection module for Okadaic acid. The differential pulse voltammograms displayed a detection limit of 8 pM with a linear range between 10—250 nM. The fabricated POCT device can be used to perform on-farm assays in fishing units.[186]

Silicon can also form as a 2D honeycomb lattice like graphene, and it is named as silicene, both forms have some structural similarities. Even though, the two differ in various aspects including the presene of most stable buckled structure of silicene instead of planar structure in graphene and non-applicable exfoliation method in silicene synthesis because this allotrope does not freely exist in nature. So, the popular method to prepare silicene is to deposit Si atoms on a metal substrate. Amorim *et al.* presented a theoretical study regarding the interaction between silicene and DNA nucleobases and suggested a possible application as a biosensor. The studies demonstrated that the thymine and adenine are physisorbed on silicene instead of guanine and cytosine, which are poorly chemisorbed *via* the formation of a Si–O bond. Besides, they studied the adsorption of DNA based on the electronic properties of silicene, explaining that it is possible to distinguish an electronic signal due to the strong interaction of guanine and cytosine with silicene from the poor interaction of adenine and thymine. The non-equillibrium Greens function method is used to explore changes in in the transmission and the conductance caused by adsorption of each nucleobase. These findings suggested that silicene could be explored as an integrated circuit biosensor as part of a LOC device for DNA sequencing.[187]

The nanomaterials integrated on the biosensors have shown better stability as well as electrical and chemical properties because the integration further amplify the sensor response which improves the selectivity and sensitivity of the biosensor. The semiconducting 2D g-C_3N_4 has displayed various advantages such as large surface area, better electrochemical reactions, excellent chemical stability, cost effectiveness and a good source of nitrogen.[188] The presence of nitrogen improves the features of electron donor/acceptor, increases the wettability with the electrolytes, together with the supply of a large additional pseudocapacitance[189] and exceptional chemical consistency. Paper electrodes are effective over screen printed electrodes as they are easily manufactured and cheaper, so making them appropriate for mass production. They do not corrode easily because they are unaffected by the conditions of the external environment, unlike the screen-printed ones. Norovirus is one of the major causes of intense diarrhoea, high fever, acute pain in the stomach and gastroenteritis. Traditional method of monitoring gave us highly promising results but had disadvantages including cost effectiveness, selectivity, sensitivity, and reduced specificity. Rana *et al.* were chosen graphitic carbon nitride (g-C_3N_4) particles for the interface of the paper electrodes. An electrochemical biosensor comprised of an electrochemical paper-based analytical device (ePAD) modified with oxidized graphitic carbon nitride (Ox-g-C_3N_4) was designed for the detection of norovirus DNA. The capture probe DNA (PDNA) modified electrodes were analyzed by CV and DPV, a limit of detection of 100 fM was observed. A non-complementary DNA was introduced on the ePAD modified using oxidized graphitic carbon nitride for testing the response of probe DNA in order to confirm the specificity of the designed biosensor. The developed ePAD sensor is simple, specific and needs a minimum analysis time of 5s.[190] The performance of microfluidic biosensors based on 2D materials is shown in Table 2.

7. Next-generation biosensors

7.1. Wearable microfluidic biosensors

Wearable biosensors have got a lot of attention from numerous fields since they allow body-worn sensors to transmit crucial data wirelessly. As a result, the Internet of Things (IoT) phenomena has spawned a plethora of opportunities. Wearables have revolutionized healthcare technology by enabling users'

Table 2 Microfluidic devices based on two-dimensional materials

Target/analyte	Detection principle	Sensing material	Substrate	LOD				Ref.
Graphene based microfluidic sensors								
Multiple biomarkers for the early detection of ovarian carcinoma	SERS	Graphene oxide	Silicon wafer	1 pg mL^{-1} and 0.01 U mL^{-1}				88
Epidermal growth factor receptor (EGFR)	CV and DPV method	Amino-functionalized graphene (NH_2-GO)/thionine (THI)/gold particle (AuNP)	Paper-based substrate	5 pg mL^{-1}				91
Pseudopodium-enriched atypical kinase one, SGK269 (PEAK1) biomarkers of pancreatic cancer	CV and DPV method	Graphene oxide	Paper-based substrate	10 pg mL^{-1}				92
microRNAs (miRNA-155 and miRNA-21) biomarkers of lung cancer	DPV	Rgo or MoS_2 nanosheet decorated with gold nanoparticles	Paper-based substrate		AuNPs/ RGO		AuNPs/ MoS_2	93
				miRNA-21	12 nM		51.6 nM	
				miRNA-155	25.7 nM		59.6 nM	
Carcinoembryonic antigen (CEA) detection	Impedance studies	Graphene-PEDOT:PSS modified	Paper based substrate	1.06 ng mL^{-1} in human serum samples				96
Carcinoma antigen 125	CV, DPV and impedance studies	Au-boron-doped graphene (BG)/boron-doped diamond (BDD) composite film	VBG/BDD	0.15 pg mL^{-1}				100
BRCA1 and BRCA2 mutation genes	Attenuated total reflection (ATR)	Graphene coated fiber-optic SPR biosensor	Fiber	—				104
ssDNA detection	Transfer characteristics	Graphene	Lab-on-printed circuit board	1 nm				110
Thrombin protein biomarker	SPR	Cys-Rgo hydrogel	PDMS	4 pg mL^{-1}				113
Glucose	Electrochemical studies	Laser induce graphene (LIG)	PET	—				118
Glucose and H_2O_2	Electrochemiluminescence (ECL)	Laser induce graphene (LIG)	PI	Glucose		H_2O_2		119
				0.138 μM		5.8729 μM		
Vitamin B12, Vitamin C and H_2O_2	Electrochemiluminescence (ECL)	Laser induce graphene (LIG)	PI	Vitamin B12	Vitamin C	H_2O_2		120
				0.109 nM	0.96 M	0.303 M		
H_2O_2, glucose, dopamine and xanthine	Electrochemiluminescence (ECL)	Laser induce graphene (LIG)	PI	H_2O_2	Glucose	Dopamine	Xanthine	121
				1.71 μM	3.76 μM	3.40 μM	1.25 μM	
D-Glucose, H_2O_2, choline and lactate	Electrochemiluminescence (ECL)	Laser induce graphene (LIG)	PI	D-Glucose	H_2O_2	Choline	Lactate	122
				2.51 μM	4.36 μM	4.01 M	5.32 μM	
Paracetamol and glucose	Impedance studies	Chitosan/GO modified PAD	Paper based substrate	—				124
Glucose	Electrochemical studies	Prussian blue-deposited rGO-tetraethylene pentamine (PB/rGO-TEPA)	Paper based substrate	25 μM				125
Glucose	Transfer characteristics	Pyrene-1-boronic acid (PBA) functionalized graphene	PDMS	0.1 μM				126
L-Lactic acid	Transfer characteristic studies	Graphene-based transistor (GFET)	PDMS	—				127
Glucose	Electrochemical studies	Graphene modified with PB	Flexible polyester sheets	—				128
Cystatin C	Electrochemical studies	GO-chitosan (GO-Chit)	Paper-based substrate	2.6 pg μL^{-1}				133
Uric acid and thyrosine	Electrochemical studies	Laser engraved graphene	Polyimide	UA		Tyr		134
				0.74 μM		3.6 μM		
Ascorbic acid	Impedance studies		PVC foil	125.01 μM				135

Table 2 (*continued*)

Target/analyte	Detection principle	Sensing material	Substrate	LOD			Ref.
SARS-CoV-2	Electrochemical transduction	Functionalized rGO nanoflakes	PDMS	2.8×10^{-15} m			138
SARS-CoV-2	Electrochemical studies			100 fg mL^{-1}			139
SARS-CoV-2	Impedance studies	Graphene/carbon ink mixture	Paper-based substrate	0.25 fg mL^{-1}			140
Hepatitis B Virus (HBV)	Amperometric detection	Screen-printed graphene electrode	PVC	0.17 μg mL^{-1}			141
Hepatitis C core antigen (HCVcAg) and hepatitis B surface antigen (HBsAg)	Electrochemical studies	Graphene	Paper-based substrate	HCVcAg	HBsAg		142
				1.19 pg mL^{-1}	18.2 pg mL^{-1}		
Sn(II) and Pb(II)	Electrochemical studies	Bismuth nanoparticles (BiNPs)/screen printed graphene electrode	Paper-based substrate	Sn(II)	Pb(II)		146
				0.26 ng mL^{-1}	0.44 ng mL^{-1},		
NO_2 gas	(RI) sensors	Graphene	On-chip	0.5 ppm			147
MXene based microfluidic sensors							
Creatinine, uric acid, and urea	Electrochemical studies	MXene/methylene blue	PMMA	Creatinine	Uric acid	Urea	17
				1.2×10^{-6} m	5×10^{-6} m	—	
Glucose and lactate	Electrochemical studies	MXene/Prussian blue (MXene/PB)	Ecoflex substrate	H_2O_2	Glucose	Lactate	150
				67×10^{-9} m	0.33×10^{-6} m	0.67×10^{-6} m	
Potassium [K^+] ion	Electrochemical studies	MXene/MWCNT	PET	—			151
Indole, odoriferous benzaldehyde and 2,4-dinitrotoluene (DNT)	SERS			Indole	DDT		153
				10 ppb	50 ppb		
TMDs based microfluidic sensors							
Salmonella typhimurium	CV and DPV	CTAB-MoS_2	PDMS	1.56 CFU mL^{-1}			174
DNA	Fluorescence	3D MoS_2/MWCNT	PDMS	1 nM			162
H_2O_2	Chronoamperometry	1T WS_2	PDMS	2.0 nM			155
MOF based microfluidic biosensors							
Glucose	Colorimetry	ZIF-8/GO_x/HRP	PP	8 μM			176
Glucose	Colorimetry	GOx Zr-PCN-222	Paper based substrate	0.25 $mmoL^{-1}$			180
PFOS	Electrochemical technique	Cr-MIL-101	PP	0.5 ng L^{-1}			211
Salmonella typhimurium	Colorimetry	NH_2-MIL-101 Fe	PDMS	14 CFU mL^{-1}			181
Other 2D materials							
Okadaic acid	DPV	Phosphene	PDMS	8 pM			186
Norovirus	CV and DPV	Ox-g-C_3N_4	Paper	100 fM			190
Microfluidic wearable biosensors based on 2D materials							
Glucose	Photodetection	MoS_2	PDMS	<0.1 mM			195
Cortisol	Electrochemical Technique	$Ti_3C_2T_x$/LBG	PDMS	—			203
Glucose Lactate	Electrochemical Technique	$Ti_3C_2T_x$/PB	Ecoflex sheet	Glucose 35.3 μA Mm^{-1} cm^{-2}	Lactate 11.4 μA Mm^{-1} cm^{-2}		202

diagnosis and prognosis through a minute collection of physiological signals, mechano-transduced forces, or body fluids. However, this is difficult to implement due to the difficulties in recovering signals from the human body. Furthermore, the high benefit requirements on body-worn sensors need them to be flexible, lightweight, and water-resistant.[191] There have been technological advancements in recent years, such as incorporating microfluidics in wearables, which are confident in their ability to overcome some of these issues. Microfluidic wearable biosensor technologies are the use of microfluidics in wearable biosensor applications. Microfluidics has numerous key-value innovations in this area. It primarily develops the sensing element's core with microstructures for liquid management or storage.[192] By allowing accurate adjustment of liquid amounts, sensing accuracy and reliability can be considerably increased. This is especially beneficial because human bodily fluids are frequently released in small quantities. In this scenario, microstructures require significantly lower liquid quantities, lowering the patient's complexity. Aside from liquid handling, microstructures can also serve as physical containers for the storage and discharge solutes at regular intervals. Furthermore, the micropatterned components can act as an electrical communication route in rigid platforms. These allow for high flexibility while maintaining high electrical conductivity in microelectromechanical systems (MEMS).[193] This highlights the novel concept of investigating microfluidic components and creating wearable microfluidics for continuous healthcare monitoring. Also graphene and graphene-like layered 2D materials such as MXenes, TMDs and MOF have gained immense importance as supporting substrates and transduction components in a wide variety of biosensing applications. The unique qualities of 2D materials, such as the high density of active sites over a vast surface, make them ideal for biosensing applications.[194] 2D materials can be tuned to display selective responses toward the target analytes with excellent sensitivity by surface chemistry modification *via* defect engineering or surface functionalization. 2D materials are an essential paradigm of nanomaterials for health care applications and next-generation biosensors because of their layer-dependent band structure and the ability to create heterostructures. 2D materials are useful for sensing applications that require high sensitivity because of their atomic thinness and large surface area, which result in a robust response to surface adsorption process. When combined with tunable band structure, desirable electrical properties, and a wide range of optical phenomena, these characteristics make 2D materials a strong contender for biosensing applications.[194]

Wearable smart contact lenses have piqued the interest of many people due to their ability to immediately monitor environmental and physiological information from the body and eyeball fluids. Smart contact lenses equipped with highly sensitive glucose sensors could pave the way for continuous non-invasive monitoring of biomarkers in tears. The integrated circuit chips or sensors must be biocompatible and stable compared to the eyeball.[195] Transparent and flexible atomically thin electronic materials, such as mono-to-few-layered 2D TMDs, could be appropriate building blocks for this application. The issue, however, lies in the selection of the manufacturing technique and the same materials. Furthermore, unlike conventional circuit chips and bulk sensors, which are often sandwiched between lens substrates and coupled to eye drops *via* microfluidic sensing ducts,[196,197] giving greater detection sensitivity and straightforward assembly without interference from blinking. Even though standard smart contact lens solutions lack biocompatibility, efficient sensor modalities, mechanical stability, and a specific fabrication method.

Contact lenses containing multifunctional sensor arrays with elastic linked nodes, PDMS lens substrate, PI passivation layers, and ultrathin TMDC semiconductors were developed to fulfill the aforementioned goals. Here, MoS_2 transistors were used as core sensing material due to their layered dangling-bond-free surface, high surface area, large surface area, good biocompatibility, charge transfer properties and tunable bandgap.[159,198–200] An Au-mediated exfoliation and assembly technique was used to create mono-to few-layered MoS_2 sheets with a lateral dimension of 200 × 100 μm. A thin film of photo patternable PI with mechanically reinforced MoS_2 transistors and the elastic parts were created using PI mesh structure and serpentine gold. The vision blocking is avoided by placing the sensor system close to the outer parts of the cornea. Mechanical analysis indicated that this design could effectively insulate devices from catastrophic mechanical deformations while maintaining high stretchability and the ability to readily transform functional components into diverse shapes of curvatures. Fig. 13a shows the structural architecture of a smart contact lens with a serpentine mesh sensor structure that is based on ultrathin MoS_2 transistors. With UV illumination, these thin MoS_2 transistors have a fast response of less than 1 s, high sensitivity (0.1 mM) and responsivity (4.8 A W^{-1}) for photodetection, and a high current on/off ratio (>103).[195] They also confirmed the contact lens system's light absorption to demonstrate transparency and performed *in vitro* cytotoxicity tests to ensure biocompatibility. Overall, the device features and material show that such contact lenses have addressed the needs for practical applications, providing a simple and new way for multipurpose contact lens sensor devices. This research creates a smart contact lens system that is very transparent, easy to use, and multipurpose. The serpentine mesh sensor device was installed directly on the lens substrate and maintained real interaction with the tears. This resulted in a more excellent performance without obstructing vision or blinking while remaining mechanically sturdy. Other functional components, such as power modules for future *in vivo* research, electrode arrangements for electroretinography, and antennae for wireless transmission, can be added more easily thanks to the fabrication technique and integrated contact lens sensor system.

Electrochemical biosensors play a significant role in sensing technologies among many wearable biosensors. Sensing electrodes plays a substantial role in the construction of wearable sensors in this technology. Advanced 2D materials, such as MXene, have replaced traditional contact surface areas and introduced appropriate electrical and mechanical properties.[201]

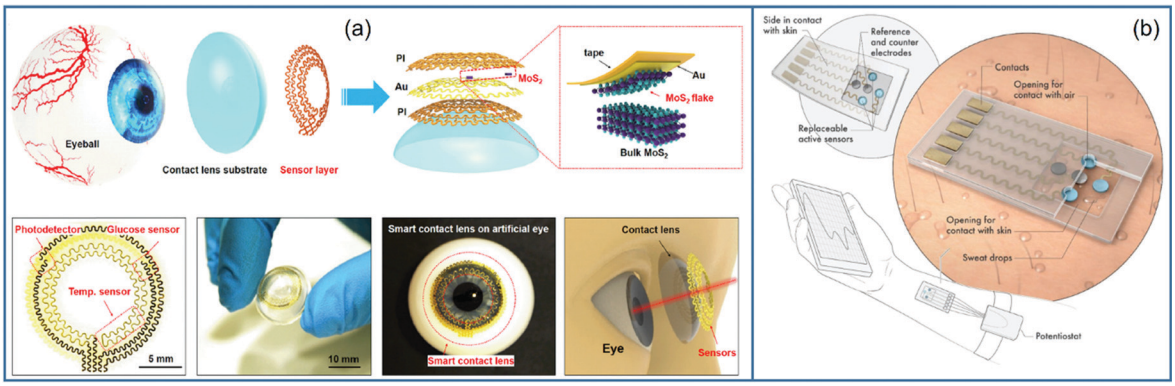

Fig. 13 (a) Structure of a smart contact lens with a serpentine mesh sensor system based on ultrathin MoS_2 transistors. Source reprinted from S. Guo, K. Wu, C. Li, H. Wang, Z. Sun, D. Xi, *et al.*, Integrated contact lens sensor system based on multifunctional ultrathin MoS_2 transistors, *Matter*., 2021, **4**(3), 969–985. (b) $Ti_3C_2T_x$/PB based glucose/lactate and pH sensor developed by Lei *et al.* (Source: reprinted from Y. Lei, W. Zhao, Y. Zhang, Q. Jiang, J.-H. He, A. J. Baeumner, O. S. Wolfbeis, Z. L. Wang, K. N. Salama and H. N. Alshareef-, A MXene-Based Wearable Biosensor System for High-Performance *In Vitro* Perspiration Analysis, *Small* 2019, 1901190, with permission from Elsevier).

Furthermore, the use of MXene in conjunction with biomarkers for microfluidic wearable electrochemical biosensors has received little attention in wearable microfluidic systems, but it is fast gaining traction In this regard, Lei *et al.* have introduced MXene-based microfluidic wearable electrochemical biosensors for sweat detection. Due to the excellent electrochemical activity and high conductivity, exfoliated MXene ($Ti_3C_2T_x$) with PB composites displayed higher electrochemical performance than graphene/PB and CNT/PB composites against H_2O_2 detection. In this case, the sensor device has a changeable sensor component that can be inserted and replaced with customized sensors designed to track various analytes such as lactate, glucose or pH value. The device substrate was composed of superhydrophobic carbon fiber to produce a tri-phase contact and protect the connector from sweat corrosion. The sensing performance of the manufactured device was evaluated using artificial sweat, and it demonstrated glucose sensitivity around 35.3 μA mm^{-1} cm^{-2} and lactate sensitivity around 11.4 μA mm^{-1} cm^{-2}.[202] Fig. 13b depicts the schematic diagram of the wearable multipurpose biosensing patch based on $Ti_3C_2T_x$/PB composite. The sensor was also tested for human sweat analysis. The test findings showed simultaneous lactate and glucose readings with great sensitivity and reproducibility. A skin-conforming flexible biosensor with three interchangeable sensor units is integrated onto a single wearable platform in the constructed system. O_2 access to the active enzymatic layer is infinite, promising intense enzyme activity and resulting inaccuracy, ultra-high sensitivity and a wider linear detection range.

Similarly, Noh *et al.* reported a new wearable impedimetric immunosensor comprising a chamber based on $Ti_3C_2T_x$-loaded LBG (laser-burned graphene) flakes 3D electrode and microfluidic channel for the non-invasive detection of cortisol in human perspiration. To create these elastic and flexible patch sensors, PDMS was used as a substrate, and LBG was placed onto the PDMS substrate by removing the PI film. When the LBG was transferred to the PDMS, a disconnection formed between the LBG flakes due to transferring and burning, which mainly influenced the electrochemical sensing response of the LBG electrode. As a result, a highly conductive MXene was introduced into the electrode, with good enzyme loading capacities and electrochemical characteristics. The microfluidic system was constructed using PDMS and a 3D-printed mold. Sweat was gathered *via* a patch sensor that was adhered to the skin with a double-sided adhesive film. Then a hole was created in the adhesive layer *via* which perspiration secreted by the skin is transmitted to the chamber under natural pressure *via* the channel. The PDMS/LBG MXene-based patch sensor had linearity and LOD around 0.01–100 Nm and 88 pM, respectively, under ideal conditions.[203] Wearable microfluidic biosensors for sweat analytics offer a viable method for detecting biomarkers without invasive testing. Nonetheless, sweat-based sensing faces several challenges, including short sensor shelf lives when using these whole working electrodes patterned using traditional techniques, easy degradation of biomaterials and enzymes with repeated tests, and limited sensitivity and detection range of enzyme-based biosensors due to sweat oxygen deficiency. The performance of microfluidic wearable biosensors based on 2D materials is shown in Table 2.

7.2. Conclusion and future directions

There are several obstacles to overcome to realize microfluidic wearable biosensors. Microstructure design and electronics functionality are two significant areas of concern. Fig. 14 depicts a schematic illustration of the general issues of wearable systems and the practical features of sensing entities. Biosensor wearability is primarily determined by materials that match human skin's biological, chemical, and physical attributes. However, difficulties arise because the human body contains uneven surfaces that are tough to remove. Human skin is also viscoelastic and very deformable. The outer epidermis layer permits fluid exchange to carry on homeostasis within the body. Finally, the adverse reaction of the epidermis towards foreign materials or chemicals, causing discomfort and skin irritation. So, the sensor material interface demands to consider all these requirements.

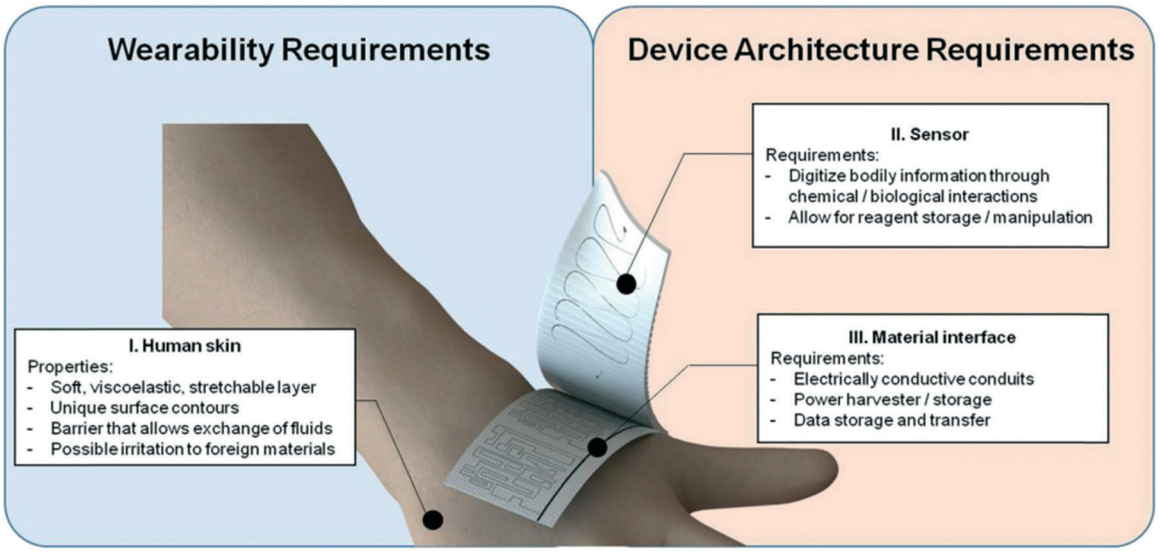

Fig. 14 Schematic representation of the broad challenges of wearable systems and the practical aspects of the sensing entities.

To summarise, skin qualities should be compatible with biosensors while achieving digitalization of bodily information *via* specialized mechanical or chemical interactions, or both. Despite the fact that many of the appealing features of microfluidics/LOC devices have enabled the use of microchip-based platforms in life science and biology, microfluidic technologies often increase the performance of existing macroscale assays or give comparable alternatives.[204] On the other hand, they have not reached their full capabilities due to a lack of new essential qualities. On the other hand, microfluidics technologies have lately been adopted to address difficulties that have not yet been addressed by the traditional laboratory tabletop method. Skin interfaced wearable biosensors used in sports analytics and wearable healthcare monitoring are one such example. Although this sector is still in its early stages, the foundations are extraordinarily strong; wearable LOC devices are gradually integrating with traditional techniques like flexible electronics, microfluidics, biocompatible materials, *etc.* Wearable biosensors are still in their developing stage with much ability for improvement in performance (accuracy, reliability, resolution, durability, limit of detection) and their sensing parameters (temperature, pressure, pH, force, hydration). Microfluidic wearable biosensors open up new avenues for improving life productivity and quality and enabling individual healthcare. Next-generation microfluidic wearables have the potential to provide unprecedented sensing, control, and monitoring capabilities. Considering these facts, we predict some potential and constraints for next-generation wearable systems for clinical applications.[205] Despite many possibilities lying ahead, several challenges need to be conquered to implement wearable microfluidic sensors for clinical biosensing applications successfully. Many issues are critical and must be addressed right now. The extended stability and endurance of different parts of wearable microfluidics, for example, have yet to be thoroughly described and presented. At the moment, the majority of the individual components of wearable microfluidic-based devices are still in the early stages of research and are constrained to the lab setting. Additional work and robust characterization are required to get beyond this early level. These individual elements must go through a series of accelerated life tests to determine whether they can resist the wear and tear associated with the continuous use of wearable gadgets. Furthermore, by combining various components of wearable microfluidic technology, completely functionalized wearable devices can be created. Specifically, this means that the entire sequence of external stimuli collection, digitalization, evaluation, and data transmission must be completed without interruption. Complete integration of numerous functions in conformable, stretchable, and flexible tiny parts is required.[193] These recent papers have highlighted a variety of prospects for microfluidic wearables along with challenges in the biosensing area. Finally, we anticipate that ongoing and progressive research in various areas, including material science, electronics, chemistry, and physics, will improve the applicability of microfluidic wearable biosensors.

Microfluidics and microfluidic wearables have enormous potential in biomedical applications such as continuous health diagnosis, monitoring, and therapy. In this paper, promising research works in sensing based on 2D materials for diverse health care and environmental applications are highlighted. We anticipate that these devices will eventually improve and prolong the quality of life of humans and, ultimately, society as a whole.

Conflicts of interest

The authors declare no conflict of interest.

Acknowledgements

This work was financially supported by the Department of Science and Technology (DST)-SERB Early Career Research

project (Grant No. ECR/2017/001850), DST-Nanomission (DST/NM/NT/2019/205(G)), Karnataka Science and Technology Promotion Society (KSTePS/VGST-RGS-F/2018-19/GRD NO. 829/315). Authors would like to acknowledge the financial support from DST (Nanomission) Govt of India (SR/NM/NS-52/2016(G)).

References

1 D. Antuña-Jiménez, G. Díaz-Díaz, M. C. Blanco-López, M. J. Lobo-Castañón, A. J. Miranda-Ordieres and P. Tuñón-Blanco, in *Molecularly Imprinted Sensors*, ed. S. Li, Y. Ge, S. A. Piletsky and J. Lunec, Elsevier, Amsterdam, 2012, pp. 1–34.
2 World Health Organization, *Guidelines for drinking-water quality*, World Health Organization, Geneva, 4th edn, 2011.
3 K. Yang, H. Peretz-Soroka, Y. Liu and F. Lin, *Lab. Chip*, 2016, **16**, 943–958.
4 R. Antony, M. S. Giri Nandagopal, N. Sreekumar and N. Selvaraju, *Microsyst. Technol.*, 2014, **20**, 1051–1061.
5 X. Chen, S. Zhang, W. Han, Z. Wu, Y. Chen and S. Wang, *J. Chem. Technol. Biotechnol.*, 2018, **93**, 3353–3363.
6 S. A. Jaywant and K. M. Arif, *Sensors*, 2019, **19**, 4781.
7 S. Gupta, K. Ramesh, S. Ahmed and V. Kakkar, *Int. J. Bio-Sci. Bio-Technol.*, 2016, **8**, 311–322.
8 H. Andersson and A. van den Berg, *Sens. Actuators, B.*, 2003, **92**, 315–325.
9 S. Mashaghi, A. Abbaspourrad, D. A. Weitz and A. M. van Oijen, *Trends Anal. Chem.*, 2016, **82**, 118–125.
10 L. Reverté, B. Prieto-Simón and M. Campàs, *Anal. Chim. Acta*, 2016, **908**, 8–21.
11 F. Ghorbani Zamani, H. Moulahoum, M. Ak, D. Odaci Demirkol and S. Timur, *TrAC, Trends Anal. Chem.*, 2019, **118**, 264–276.
12 S. Wu, X. Wang, Z. Li, S. Zhang and F. Xing, *Micromachines*, 2020, **11**, 1059.
13 J. Kudr, O. Zitka, M. Klimanek, R. Vrba and V. Adam, *Sens. Actuators, B*, 2017, **246**, 578–590.
14 R. J. Toh, C. C. Mayorga-Martinez, J. Han, Z. Sofer and M. Pumera, Group 6 Layered Transition-Metal Dichalcogenides in Lab-on-a-Chip Devices, https://pubs.acs.org/doi/pdf/10.1021/acs.analchem.7b00302, accessed 9 September 2021.
15 J. Sengupta and C. M. Hussain, *TrAC, Trends Anal. Chem.*, 2019, **114**, 326–337.
16 Y. Huang, Y. Shi, H. Y. Yang and Y. Ai, *Nanoscale*, 2015, **7**, 2245–2249.
17 J. Liu, X. Jiang, R. Zhang, Y. Zhang, L. Wu, W. Lu, J. Li, Y. Li and H. Zhang, *Adv. Funct. Mater.*, 2019, **29**, 1807326.
18 Scottish Graphene Firm Launches Flagship Product Under New Face, https://www.printedelectronicsworld.com/articles/22141/scottish-graphene-firm-launches-flagship-product-under-new-face, accessed 11 September 2021.
19 V. V. Pokropivny and V. V. Skorokhod, *Mater. Sci. Eng. C*, 2007, **27**, 990–993.
20 D. Tyagi, H. Wang, W. Huang, L. Hu, Y. Tang, Z. Guo, Z. Ouyang and H. Zhang, *Nanoscale*, 2020, **12**, 3535–3559.
21 C. N. R. Rao, A. K. Sood, K. S. Subrahmanyam and A. Govindaraj, *Angew. Chem., Int. Ed.*, 2009, **48**, 7752–7777.
22 C. Anichini, W. Czepa, D. Pakulski, A. Aliprandi, A. Ciesielski and P. Samorì, *Chem. Soc. Rev.*, 2018, **47**, 4860–4908.
23 D. J. Late, Y. K. Huang, B. Liu, J. Acharya, S. N. Shirodkar, J. Luo, A. Yan, D. Charles, U. V. Waghmare, V. P. Dravid and C. N. R. Rao, *ACS Nano*, 2013, **7**, 4879–4891.
24 X. Liu, T. Ma, N. Pinna and J. Zhang, *Adv. Funct. Mater.*, 2017, **27**, 1–30.
25 S. Xu, Z. Yan, K. I. Jang, W. Huang, H. Fu, J. Kim, Z. Wei, M. Flavin, J. McCracken, R. Wang, A. Badea, Y. Liu, D. Xiao, G. Zhou, J. Lee, H. U. Chung, H. Cheng, W. Ren, A. Banks, X. Li, U. Paik, R. G. Nuzzo, Y. Huang, Y. Zhang and J. A. Rogers, *Science*, 2015, **347**, 154–159.
26 K. S. Kumar, N. Choudhary, Y. Jung and J. Thomas, *ACS Energy Lett.*, 2018, **3**, 482–495.
27 N. Convery and N. Gadegaard, *Micro Nano Eng.*, 2019, **2**, 76–91.
28 H. A. Stone, A. D. Stroock and A. Ajdari, *Annu. Rev. Fluid Mech.*, 2004, **36**, 381–411.
29 L. Baharudin, *Instrum. Sci. Technol.*, 2008, **36**, 222–230.
30 J. Wu and M. Gu, *J. Biomed. Opt.*, 2011, **16**, 080901.
31 G. A. Schultz, T. N. Corso, S. J. Prosser and S. Zhang, *Anal. Chem.*, 2000, **72**, 4058–4063.
32 L. Licklider, X.-Q. Wang, A. Desai, Y.-C. Tai and T. D. Lee, *Anal. Chem.*, 2000, **72**, 367–375.
33 J. Kameoka, R. Orth, B. Ilic, D. Czaplewski, T. Wachs and H. G. Craighead, *Anal. Chem.*, 2002, **74**, 5897–5901.
34 B. M. D. C. Costa, S. Griveau, F. d'Orlye, F. Bedioui, J. A. F. da Silva and A. Varenne, *Electrochim. Acta*, 2021, **391**, 138928.
35 W. Cha, Y.-C. Tung, M. E. Meyerhoff and S. Takayama, *Anal. Chem.*, 2010, **82**, 3300–3305.
36 M. Bauer, L. Wunderlich, F. Weinzierl, Y. Lei, A. Duerkop, H. N. Alshareef and A. J. Baeumner, *Anal. Bioanal. Chem.*, 2021, **413**, 763–777.
37 D. Ross, M. Gaitan and L. E. Locascio, *Anal. Chem.*, 2001, **73**, 4117–4123.
38 A. Q. Liu, H. J. Huang, L. K. Chin, Y. F. Yu and X. C. Li, *Anal. Bioanal. Chem.*, 2008, **391**, 2443–2452.
39 O. Tamarin, S. Comeau, C. Déjous, D. Moynet, D. Rebière, J. Bezian and J. Pistré, *Biosens. Bioelectron.*, 2003, **18**, 755–763.
40 B. Godber, K. S. J. Thompson, M. Rehak, Y. Uludag, S. Kelling, A. Sleptsov, M. Frogley, K. Wiehler, C. Whalen and M. A. Cooper, *Clin. Chem.*, 2005, **51**, 1962–1972.
41 L.-S. Bouchard, S. R. Burt, M. S. Anwar, K. V. Kovtunov, I. V. Koptyug and A. Pines, *Science*, 2008, **319**, 442–445.
42 V.-V. Telkki, C. Hilty, S. Garcia, E. Harel and A. Pines, *J. Phys. Chem. B*, 2007, **111**, 13929–13936.
43 M. Mujika, S. Arana, E. Castaño, M. Tijero, R. Vilares, J. M. Ruano-López, A. Cruz, L. Sainz and J. Berganza, *Biosens. Bioelectron.*, 2009, **24**, 1253–1258.

44 G. Minas, J. S. Martins, J. C. Ribeiro, R. F. Wolffenbuttel and J. H. Correia, *Sens. Actuators Phys.*, 2004, **110**, 33–38.
45 B. Filanoski, S. K. Rastogi, E. Cameron, N. N. Mishra, W. Maki and G. Maki, *Luminescence*, 2008, **23**, 22–27.
46 O. Hofmann, P. Miller, P. Sullivan, T. S. Jones, J. C. deMello, D. D. C. Bradley and A. J. deMello, *Sens. Actuators, B*, 2005, **106**, 878–884.
47 A. M. Jorgensen, K. B. Mogensen, J. P. Kutter and O. Geschke, *Sens. Actuators, B*, 2003, **90**, 15–21.
48 W. K. Ridgeway, E. Seitaridou, R. Phillips and J. R. Williamson, *Nucleic Acids Res.*, 2009, **37**, e142.
49 J. G. Santiago, S. T. Wereley, C. D. Meinhart, D. J. Beebe and R. J. Adrian, *Exp. Fluids*, 1998, **25**, 316–319.
50 M. G. Olsen, J. M. Bauer and D. J. Beebe, *Appl. Phys. Lett.*, 2000, **76**, 3310–3312.
51 D. Sinton, R. Gordon and A. G. Brolo, *Microfluid. Nanofluidics*, 2008, **4**, 107–116.
52 A. De Leebeeck, L. K. S. Kumar, V. de Lange, D. Sinton, R. Gordon and A. G. Brolo, *Anal. Chem.*, 2007, **79**, 4094–4100.
53 I. T. Kim and K. D. Kihm, *Exp. Fluids*, 2006, **41**, 905–916.
54 D. J. Sirbuly, A. Tao, M. Law, R. Fan and P. Yang, *Adv. Mater.*, 2007, **19**, 61–66.
55 P. Dumais, C. L. Callender, J. P. Noad and C. J. Ledderhof, *Opt. Express*, 2008, **16**, 18164–18172.
56 R. G. Heideman and P. V. Lambeck, *Sens. Actuators, B*, 1999, **61**, 100–127.
57 J. A. Chediak, Z. Luo, J. Seo, N. Cheung, L. P. Lee and T. D. Sands, *Sens. Actuators Phys.*, 2004, **111**, 1–7.
58 K. R. Strehle, D. Cialla, P. Rösch, T. Henkel, M. Köhler and J. Popp, *Anal. Chem.*, 2007, **79**, 1542–1547.
59 B. D. Piorek, S. J. Lee, J. G. Santiago, M. Moskovits, S. Banerjee and C. D. Meinhart, *Proc. Natl. Acad. Sci. U. S. A.*, 2007, **104**, 18898–18901.
60 J. C. Fanguy and C. S. Henry, *Electrophoresis*, 2002, **23**, 767–773.
61 W. Cha, Y.-C. Tung, M. E. Meyerhoff and S. Takayama, *Anal. Chem.*, 2010, **82**, 3300–3305.
62 M. Bauer, L. Wunderlich, F. Weinzierl, Y. Lei, A. Duerkop, H. N. Alshareef and A. J. Baeumner, *Anal. Bioanal. Chem.*, 2021, **413**, 763–777.
63 M. Galloway, W. Stryjewski, A. Henry, S. M. Ford, S. Llopis, R. L. McCarley and S. A. Soper, *Anal. Chem.*, 2002, **74**, 2407–2415.
64 M. Žúborová, Z. Demianová, D. Kaniansky, M. Masár and B. Stanislawski, *J. Chromatogr. A*, 2003, **990**, 179–188.
65 R. H. Liu, J. Yang, R. Lenigk, J. Bonanno and P. Grodzinski, *Anal. Chem.*, 2004, **76**, 1824–1831.
66 Mass Spectrometry, https://www.wiley.com/en-gb/Mass+Spectrometry%3A+Principles+and+Applications%2C+3rd+Edition-p-9780470033104, accessed 27 December 2021.
67 D. F. Hunt, J. R. Yates, J. Shabanowitz, S. Winston and C. R. Hauer, *Proc. Natl. Acad. Sci. U. S. A.*, 1986, **83**, 6233–6237.
68 G. A. Schultz, T. N. Corso, S. J. Prosser and S. Zhang, *Anal. Chem.*, 2000, **72**, 4058–4063.
69 L. Licklider, X.-Q. Wang, A. Desai, Y.-C. Tai and T. D. Lee, *Anal. Chem.*, 2000, **72**, 367–375.
70 H. Gao, C. Yan, W. Wu and J. Li, *Sensors*, 2020, **20**, 1792.
71 P. Pattanayak, S. K. Singh, M. Gulati, S. Vishwas, B. Kapoor, D. K. Chellappan, K. Anand, G. Gupta, N. K. Jha, P. K. Gupta, P. Prasher, K. Dua, H. Dureja, D. Kumar and V. Kumar, *Microfluid. Nanofluidics*, 2021, **25**, 99.
72 Y. Zhang, J. Qi, F. Liu, N. Wang, X. Sun, R. Cui, J. Yu, J. Ye, P. Liu, B. Li and L. Chen, *Se Pu Chin. J. Chromatogr.*, 2021, **39**, 802–815.
73 J. Mairhofer, K. Roppert and P. Ertl, *Sensors*, 2009, **9**, 4804–4823.
74 C. N. R. Rao, K. Gopalakrishnan and U. Maitra, *ACS Appl. Mater. Interfaces*, 2015, **7**, 7809–7832.
75 J. Sengupta and C. M. Hussain, *TrAC, Trends Anal. Chem.*, 2019, **114**, 326–337.
76 E. W. Hill, A. Vijayaragahvan and K. Novoselov, *IEEE Sens. J.*, 2011, **11**, 3161–3170.
77 O. Moldovan, B. Iñiguez, M. J. Deen and L. F. Marsal, *IET Circuits Dev. Syst.*, 2015, **9**, 446–453.
78 E. M. Materón, R. S. Lima, N. Joshi, F. M. Shimizu and O. N. Oliveira, in *Graphene-Based Electrochemical Sensors for Biomolecules*, ed. A. Pandikumar and P. Rameshkumar, Elsevier, 2019, pp. 321–336.
79 X. Chen, S. Zhang, W. Han, Z. Wu, Y. Chen and S. Wang, *J. Chem. Technol. Biotechnol.*, 2018, **93**, 3353–3363.
80 S. Wu, X. Wang, Z. Li, S. Zhang and F. Xing, *Micromachines*, 2020, **11**, 1–25.
81 Green Synthesis of Graphene Based Biomaterial Using Fenugreek Seeds for Lipid Detection|ACS Sustainable Chemistry & Engineering, DOI: 10.1021/acssuschemeng.5b00923, accessed 17 May 2021.
82 A. C. Q. Silva, C. Vilela, H. A. Santos, A. J. D. Silvestre and C. S. R. Freire, *Appl. Mater. Today*, 2020, **18**, 100450.
83 J. L. Garcia-Cordero and S. J. Maerkl, *Curr. Opin. Biotechnol.*, 2020, **65**, 37–44.
84 C. Chircov, A. C. Bîrcă, A. M. Grumezescu and E. Andronescu, *Molecules*, 2020, **25**, 6013.
85 Y.-E. Choi, J.-W. Kwak and J. W. Park, *Sensors*, 2010, **10**, 428–455.
86 Visual and high-throughput detection of cancer cells using a graphene oxide-based FRET aptasensing microfluidic chip - Lab on a Chip (RSC Publishing), https://pubs.rsc.org/en/content/articlelanding/2012/lc/c2lc40564d#!divAbstract, accessed 22 May 2021.
87 Paper-Based Microfluidic Electrochemical Immunodevice Integrated with Nanobioprobes onto Graphene Film for Ultrasensitive Multiplexed Detection of Cancer Biomarkers|Analytical Chemistry, DOI: 10.1021/ac401445a, accessed 24 May 2021.
88 Y. Wu, C. Wang, P. Wang, C. Wang, Y. Zhang and L. Han, *RSC Adv.*, 2021, **11**, 8124–8133.
89 Z. Niu, M. A. Kozminsky, K. C. Day, P. L. Palmbos, M. L. Day and S. Nagrath, *Poster Presentations - Proffered Abstracts*, American Association for Cancer Research, 2020, p. B35.

90 Y. An, T. Jin, Y. Zhu, F. Zhang and P. He, *Biosens. Bioelectron.*, 2019, **142**, 111503.
91 Y. Wang, S. Sun, J. Luo, Y. Xiong, T. Ming, J. Liu, Y. Ma, S. Yan, Y. Yang, Z. Yang, J. Reboud, H. Yin, J. M. Cooper and X. Cai, *Microsyst. Nanoeng.*, 2020, **6**, 1–9.
92 K. S. Prasad, X. Cao, N. Gao, Q. Jin, S. T. Sanjay, G. Henao-Pabon and X. Li, *Sens. Actuators, B*, 2020, **305**, 127516.
93 H. Torul, E. Yarali, E. Eksin, A. Ganguly, J. Benson, U. Tamer, P. Papakonstantinou and A. Erdem, *Biosensors*, 2021, **11**, 236.
94 A. N. Bhatt, R. Mathur, A. Farooque, A. Verma and B. S. Dwarakanath, *Ind. J. Med. Res.*, 2010, **132**, 129–149.
95 S. Hammarström, *Semin. Cancer Biol.*, 1999, **9**, 67–81.
96 Y.-K. Yen, C.-H. Chao and Y.-S. Yeh, *Sensors*, 2020, **20**, 1372.
97 B. Guo, L. Fang, B. Zhang and J. R. Gong, *Insci. J.*, 2011, 80–89.
98 V. V. Chaban and O. V. Prezhdo, *Nanoscale*, 2016, **8**, 15521–15528.
99 S. Agnoli and M. Favaro, *J. Mater. Chem. A*, 2016, **4**, 5002–5025.
100 H. Li, J. Qin, M. Li, C. Li, S. Xu, L. Qian and B. Yang, *Sens. Actuators, B*, 2020, **302**, 127209.
101 C.-W. Lin and C.-C. Chang, *Biosens. Cancer*, 2011, 17.
102 Y. Li, A. W. Wark, H. J. Lee and R. M. Corn, *Anal. Chem.*, 2006, **78**, 3158–3164.
103 D. T. Nurrohman and N.-F. Chiu, *Nanomaterials*, 2021, **11**, 216.
104 M. B. Hossain, M. M. Islam, L. F. Abdulrazak, M. M. Rana, T. B. A. Akib and M. Hassan, *Photonic Sens.*, 2020, **10**, 67–79.
105 D. Moschou and A. Tserepi, *Lab. Chip*, 2017, **17**, 1388–1405.
106 Y.-J. Chang and H. You, *Chin. J. Anal. Chem.*, 2019, **47**, 965–975.
107 N. C. S. Vieira, J. Borme, G. Machado Jr., F. Cerqueira, P. P. Freitas, V. Zucolotto, N. M. R. Peres and P. Alpuim, *J. Phys.: Condens. Matter*, 2016, **28**, 085302.
108 F. Chen, Q. Qing, J. Xia and N. Tao, *Chem. – Asian J.*, 2010, **5**, 2144–2153.
109 Measurement of the quantum capacitance of graphene|-Nature Nanotechnology, https://www.nature.com/articles/nnano.2009.177, accessed 20 July 2021.
110 S. Papamatthaiou, P. Estrela and D. Moschou, *Sci. Rep.*, 2021, **11**, 9815.
111 G. Saltzgaber, P. Wojcik, T. Sharf, M. R. Leyden, J. L. Wardini, C. A. Heist, A. A. Adenuga, V. T. Remcho and E. D. Minot, *Nanotechnology*, 2013, **24**, 355502.
112 Y. Wang, Y. Xiao, G. Gao, J. Chen, R. Hou, Q. Wang, L. Liu and J. Fu, *J. Mater. Chem. B*, 2017, **5**, 511–516.
113 N. Singh, M. A. Ali, P. Rai, I. Ghori, A. Sharma, B. D. Malhotra and R. John, *Lab. Chip*, 2020, **20**, 760–777.
114 M. Asif, A. Aziz, M. Azeem, Z. Wang, G. Ashraf, F. Xiao, X. Chen and H. Liu, *Adv. Colloid Interface Sci.*, 2018, **262**, 21–38.
115 S. Dong, A. Q. Dao, B. Zheng, Z. Tan, C. Fu, H. Liu and F. Xiao, *Electrochim. Acta*, 2015, **C**, 195–201.
116 Z. Wang, M. Gui, M. Asif, Y. Yu, S. Dong, H. Wang, W. Wang, F. Wang, F. Xiao and H. Liu, *Nanoscale*, 2018, **10**, 6629–6638.
117 Sensors|Free Full-Text|Electrochemical Detection of Glucose Molecules Using Laser-Induced Graphene Sensors: A Review, https://www.mdpi.com/1424-8220/21/8/2818, accessed 24 July 2021.
118 P. Rewatkar, A. Kothuru and S. Goel, *IEEE Trans. Electron. Dev.*, 2020, **67**, 1832–1838.
119 M. Bhaiyya, P. Rewatkar, M. Salve, P. K. Pattnaik and S. Goel, *IEEE Trans. NanoBiosci.*, 2021, **20**, 79–85.
120 M. Bhaiyya, P. K. Pattnaik and S. Goel, *Sens. Actuators, Phys.*, 2021, **331**, 112831.
121 M. L. Bhaiyya, P. K. Pattnaik and S. Goel, *IEEE Trans. Instrum. Meas.*, 2021, **70**, 1–8.
122 M. Bhaiyya, P. K. Pattnaik and S. Goel, *IEEE Trans. Electron. Dev.*, 2021, **68**, 2447–2454.
123 Roekmono, H. Hadi, H. N. Imtihani and R. A. Wahyuono, *Int. J. Drug Delivery Technology*, 2020, **10**, 295–300.
124 L. Cao, G.-C. Han, H. Xiao, Z. Chen and C. Fang, *Anal. Chim. Acta*, 2020, **1096**, 34–43.
125 Graphene Field Effect Transistors for Biomedical Applications: Current Status and Future Prospects - PubMed, https://pubmed.ncbi.nlm.nih.gov/28933752/, accessed 1 August 2021.
126 Y. Zhi, J. Jian, Y. Qiao, Y. Tian, Y. Yang and T.-L. Ren, 2020 21st International Conference on Electronic Packaging Technology (ICEPT), 2020, pp. 1–6.
127 A. Wiorek, M. Parrilla, M. Cuartero and G. A. Crespo, *Anal. Chem.*, 2020, **92**, 10153–10161.
128 S. J. Fishlock, G. Bhattacharya and J. McLaughlin, *ECS Meet. Abstr.*, 2020, **MA2020-01**, 2347.
129 A. Schuck, H. E. Kim, J. K. Moreira, P. S. Lora and Y.-S. Kim, *Sensors*, 2021, **21**, 1852.
130 J. S. C. Chew, M. Saleem, C. M. Florkowski and P. M. George, *Clin. Biochem. Rev.*, 2008, **29**, 47–62.
131 G. Kaur and E. Levy, *Front. Mol. Neurosci.*, 2012, **5**, 79.
132 M. H. Gozashti, A. Gholamhosseinian, F. Musavi and M. Mashrouteh, *Iran. J. Reprod. Med.*, 2013, **11**, 71–76.
133 K. S. S. Devi and U. M. Krishnan, *Microchim. Acta*, 2020, **187**, 585.
134 [PDF] A laser-engraved wearable sensor for sensitive detection of uric acid and tyrosine in sweat|Semantic Scholar, https://www.semanticscholar.org/paper/A-laser-engraved-wearable-sensor-for-sensitive-of-Yang-Song/fbdbc1416c9f3cbcadbfad7131c5a1c5acc69a60#citing-papers, accessed 11 August 2021.
135 G. M. Stojanović, T. Kojić, M. Simić, A. Jovanović-Galović, B. Pavlović, A. Zurutuza, L. Anzi and R. Sordan, *IEEE Sens. J.*, 2021, **21**, 16744–16753.
136 A. E. Moutaouakil, S. Poovathy, M. Belmoubarik and W. K. Peng, *Phys.*, 2020, arXiv:2006.11881.
137 J. Sengupta, A. Adhikari and C. M. Hussain, *Carbon Trends*, 2021, **4**, 100072.
138 M. A. Ali, C. Hu, S. Jahan, B. Yuan, M. S. Saleh, E. Ju, S.-J. Gao and R. Panat, *Adv. Mater. Deerfield Beach Fla*, 2021, **33**, e2006647.

139 S. Damiati, S. Søpstad, M. Peacock, A. S. Akhtar, I. Pinto, R. R. G. Soares and A. Russom, *IEEE Sens. J.*, 2021, **21**, 13060–13067.
140 M. A. Ehsan, S. A. Khan and A. Rehman, *Diagnostics*, 2021, **11**, 1030.
141 P. Teengam, W. Siangproh, S. Tontisirin, A. Jirasereeamornkun, N. Chuaypen, P. Tangkijvanich, C. S. Henry, N. Ngamrojanavanich and O. Chailapakul, *Sens. Actuators, B*, 2021, **326**, 128825.
142 S. Boonkaew, A. Yakoh, N. Chuaypen, P. Tangkijvanich, S. Rengpipat, W. Siangproh and O. Chailapakul, *Biosens. Bioelectron.*, 2021, **193**, 113543.
143 M. Pumera, A. Ambrosi, A. Bonanni, E. L. K. Chng and H. L. Poh, *TrAC, Trends Anal. Chem.*, 2010, **29**, 954–965.
144 Chemically Modified Graphenes as Detectors in Lab-on-Chip Device - Chua - 2013 - Electroanalysis - Wiley Online Library, https://analyticalsciencejournals.onlinelibrary.wiley.com/doi/10.1002/elan.201200583, accessed 22 August 2021.
145 C. K. Chua and M. Pumera, *Electrophoresis*, 2013, **34**, 2007–2010.
146 K. Pungjunun, S. Nantaphol, N. Praphairaksit, W. Siangproh, S. Chaiyo and O. Chailapakul, *Sens. Actuators, B*, 2020, **318**, 128241.
147 J. Wang, X. Zhang, Z. Wei, H. Qiu, Y. Chen, Y. Geng, Y. Du, Z. Cheng and X. Li, *IEEE Access*, 2021, **9**, 56479–56485.
148 R. A. Soomro, S. Jawaid, Q. Zhu, Z. Abbas and B. Xu, *Chin. Chem. Lett.*, 2020, **31**, 922–930.
149 Y. Lei, W. Zhao, Y. Zhang, Q. Jiang, J.-H. He, A. J. Baeumner, O. S. Wolfbeis, Z. L. Wang, K. N. Salama and H. N. Alshareef, *Small*, 2019, **15**, 1901190.
150 M. Li, L. Wang, R. Liu, J. Li, Q. Zhang, G. Shi, Y. Li, C. Hou and H. Wang, *Biosens. Bioelectron.*, 2021, **174**, 112828.
151 S. Zhang, M. A. Zahed, M. Sharifuzzaman, S. Yoon, X. Hui, S. Chandra Barman, S. Sharma, H. S. Yoon, C. Park and J. Y. Park, *Biosens. Bioelectron.*, 2021, **175**, 112844.
152 M. M. Tunesi, R. A. Soomro, X. Han, Q. Zhu, Y. Wei and B. Xu, *Nano Converg.*, 2021, **8**, 5.
153 K. Yang, K. Zhu, Y. Wang, Z. Qian, Y. Zhang, Z. Yang, Z. Wang, L. Wu, S. Zong and Y. Cui, *ACS Nano*, 2021, **15**, 12996–13006.
154 P. Yager, T. Edwards, E. Fu, K. Helton, K. Nelson, M. R. Tam and B. H. Weigl, *Nature*, 2006, **442**, 412–418.
155 R. J. Toh, C. C. Mayorga-Martinez, J. Han, Z. Sofer and M. Pumera, *Anal. Chem.*, 2017, **89**, 4978–4985.
156 S. He, B. Song, D. Li, C. Zhu, W. Qi, Y. Wen, L. Wang, S. Song, H. Fang and C. Fan, *Adv. Funct. Mater.*, 2010, **20**, 453–459.
157 S. Song, Z. Liang, J. Zhang, L. Wang, G. Li and C. Fan, *Angew. Chem., Int. Ed.*, 2009, **48**, 8670–8674.
158 R. Yang, J. Jin, Y. Chen, N. Shao, H. Kang, Z. Xiao, Z. Tang, Y. Wu, Z. Zhu and W. Tan, *J. Am. Chem. Soc.*, 2008, **130**, 8351–8358.
159 C. Zhu, Z. Zeng, H. Li, F. Li, C. Fan and H. Zhang, *J. Am. Chem. Soc.*, 2013, **135**, 5998–6001.
160 P. T. K. Loan, W. Zhang, C.-T. Lin, K.-H. Wei, L.-J. Li and C.-H. Chen, *Adv. Mater.*, 2014, **26**, 4838–4844.
161 D. Ren, H. Jiang, Y. Hu, L. Zhang and C. Li, *RSC Adv.*, 2014, **4**, 40368–40372.
162 D. Yang, M. Tayebi, Y. Huang, H. Y. Yang and Y. Ai, *Sensors*, 2016, **16**, 1911.
163 S.-K. Eng, P. Pusparajah, N.-S. Ab Mutalib, H.-L. Ser, K.-G. Chan and L.-H. Lee, *Front. Life Sci.*, 2015, **8**, 284–293.
164 F. Adzitey, N. Huda and G. R. R. Ali, *3 Biotechnol.*, 2013, **3**, 97–107.
165 X. Ni, M. Castanares, A. Mukherjee and S. E. Lupold, *Curr. Med. Chem.*, 2011, **18**, 4206–4214.
166 D. Chimene, D. L. Alge and A. K. Gaharwar, *Adv. Mater.*, 2015, **27**, 7261–7284.
167 H.-L. Shuai, X. Wu and K.-J. Huang, *J. Mater. Chem. B*, 2017, **5**, 5362–5372.
168 D. Sarkar, W. Liu, X. Xie, A. C. Anselmo, S. Mitragotri and K. Banerjee, *ACS Nano*, 2014, **8**, 3992–4003.
169 S. Z. Butler, S. M. Hollen, L. Cao, Y. Cui, J. A. Gupta, H. R. Gutiérrez, T. F. Heinz, S. S. Hong, J. Huang, A. F. Ismach, E. Johnston-Halperin, M. Kuno, V. V. Plashnitsa, R. D. Robinson, R. S. Ruoff, S. Salahuddin, J. Shan, L. Shi, M. G. Spencer, M. Terrones, W. Windl and J. E. Goldberger, *ACS Nano*, 2013, **7**, 2898–2926.
170 Y.-C. Lin, D. O. Dumcenco, Y.-S. Huang and K. Suenaga, *Nat. Nanotechnol.*, 2014, **9**, 391–396.
171 C. N. R. Rao, H. S. S. R. Matte and U. Maitra, *Angew. Chem., Int. Ed.*, 2013, **52**, 13162–13185.
172 A. H. Loo, A. Bonanni, A. Ambrosi and M. Pumera, *Nanoscale*, 2014, **6**, 11971–11975.
173 K.-J. Huang, Y.-J. Liu, H.-B. Wang, Y.-Y. Wang and Y.-M. Liu, *Biosens. Bioelectron.*, 2014, **55**, 195–202.
174 C. Singh, M. A. Ali, V. Kumar, R. Ahmad and G. Sumana, 2017, **259**, DOI: 10.1016/J.SNB.2017.12.094.
175 S. Nagabooshanam, S. Roy, A. Mathur, I. Mukherjee, S. Krishnamurthy and L. M. Bharadwaj, *Sci. Rep.*, 2019, **9**, 19862.
176 M. Mohammad, A. Razmjou, K. Liang, M. Asadnia and V. Chen, *ACS Appl. Mater. Interfaces*, 2019, **11**, 1807–1820.
177 A. W. Martinez, S. T. Phillips, E. Carrilho, S. W. Thomas, H. Sindi and G. M. Whitesides, *Anal. Chem.*, 2008, **80**, 3699–3707.
178 D. A. Bruzewicz, M. Reches and G. M. Whitesides, *Anal. Chem.*, 2008, **80**, 3387–3392.
179 A. W. Martinez, S. T. Phillips, B. J. Wiley, M. Gupta and G. M. Whitesides, *Lab. Chip*, 2008, **8**, 2146–2150.
180 G. C. Ilacas, A. Basa, K. J. Nelms, J. D. Sosa, Y. Liu and F. A. Gomez, *Anal. Chim. Acta*, 2019, **1055**, 74–80.
181 W. Qi, L. Zheng, S. Wang, F. Huang, Y. Liu, H. Jiang and J. Lin, *Biosens. Bioelectron.*, 2021, **178**, 113020.
182 L. Chen, D. W. McBranch, H. L. Wang, R. Helgeson, F. Wudl and D. G. Whitten, *Proc. Natl. Acad. Sci. U. S. A.*, 1999, **96**, 12287–12292.
183 S. Chatterjee, M. S. Fujimoto, Y. H. Cheng, R. Kargupta, J. A. Soltis, R. K. Motkuri and S. Basuray, *Sens. Actuators, B*, 2019, **284**, 663–674.
184 Y. H. Cheng, D. Barpaga, J. A. Soltis, V. Shutthanandan, R. Kargupta, K. S. Han, B. P. McGrail, R. K. Motkuri,

S. Basuray and S. Chatterjee, *ACS Appl. Mater. Interfaces*, 2020, **12**, 10503–10514.
185 A. Jayakumar, A. Surendranath and M. Pv, *Int. J. Pharm.*, 2018, **551**, 309–321.
186 S. Ramalingam, R. Chand, C. B. Singh and A. Singh, *Biosens. Bioelectron.*, 2019, **135**, 14–21.
187 R. G. Amorim and R. H. Scheicher, *Nanotechnology*, 2015, **26**, 154002.
188 E. Hu, J. Ning, B. He, Z. Li, C. Zheng, Y. Zhong, Z. Zhang and Y. Hu, *J. Mater. Chem. A*, 2017, **5**, 2271–2279.
189 Simple and Large Scale Construction of MoS_2-g-C_3N_4 Heterostructures Using Mechanochemistry for High Performance Electrochemical Supercapacitor and Visible Light Photocatalytic Applications|Scientific Reports, https://www.nature.com/articles/srep43055#Abs1, accessed 31 December 2021.
190 A. Rana, M. Killa, N. Yadav, A. Mishra, A. Mathur, A. Kumar, M. Khanuja, J. Narang and R. Pilloton, *Sensors*, 2020, **20**, 2070.
191 W. Gao, S. Emaminejad, H. Y. Y. Nyein, S. Challa, K. Chen, A. Peck, H. M. Fahad, H. Ota, H. Shiraki, D. Kiriya, D.-H. Lien, G. A. Brooks, R. W. Davis and A. Javey, *Nature*, 2016, **529**, 509–514.
192 J. Guo, Y. Yu, L. Cai, Y. Wang, K. Shi, L. Shang, J. Pan and Y. Zhao, *Mater. Today*, 2021, **44**, 105–135.
193 Y. Yu, X. Wang, C. Yang and L. Shang, *Lab. Chip*, 2016, **16**, 4082–4090.
194 A. Bolotsky, D. Butler, C. Dong, K. Gerace, N. R. Glavin, C. Muratore, J. A. Robinson and A. Ebrahimi, *ACS Nano*, 2019, **13**, 9781–9810.
195 S. Guo, K. Wu, C. Li, H. Wang, Z. Sun, D. Xi, S. Zhang, W. Ding, M. E. Zaghloul, C. Wang, F. A. Castro, D. Yang and Y. Zhao, *Matter*, 2021, **4**, 969–985.
196 N. Jiang, Y. Montelongo, H. Butt and A. K. Yetisen, *Small*, 2018, **14**, 1704363.
197 T. Kamei and T. Wada, *Appl. Phys. Lett.*, 2006, **89**, 114101.
198 S. Luo, S. Wu, J. Xu, X. Zhang, L. Zou, R. Yao, L. Jin and Y. Li, *Appl. Nanosci.*, 2020, **10**, 3703–3716.
199 O. Lopez-Sanchez, D. Lembke, M. Kayci, A. Radenovic and A. Kis, *Nat. Nanotechnol.*, 2013, **8**, 497–501.
200 A. Shokri and N. Salami, *Sens. Actuators, B*, 2016, **236**, 378–385.
201 J. S. Nah, S. C. Barman, M. A. Zahed, M. Sharifuzzaman, H. Yoon, C. Park, S. Yoon, S. Zhang and J. Y. Park, *Sens. Actuators, B*, 2021, **329**, 129206.
202 Y. Lei, W. Zhao, Y. Zhang, Q. Jiang, J.-H. He, A. J. Baeumner, O. S. Wolfbeis, Z. L. Wang, K. N. Salama and H. N. Alshareef, *Small*, 2019, **15**, 1901190.
203 J. S. Nah, S. C. Barman, M. A. Zahed, M. Sharifuzzaman, H. Yoon, C. Park, S. Yoon, S. Zhang and J. Y. Park, *Sens. Actuators, B*, 2021, **329**, 129206.
204 J. C. Yeo, Kenry and C. T. Lim, *Lab. Chip*, 2016, **16**, 4082–4090.
205 A. Sharma, M. Badea, S. Tiwari and J. L. Marty, *Molecules*, 2021, **26**, 748.
206 T. W. Odom, J. C. Love, D. B. Wolfe, K. E. Paul and G. M. Whitesides, *Langmuir*, 2002, **18**, 5314–5320.
207 H. Cao, J. O. Tegenfeldt, R. H. Austin and S. Y. Chou, *Appl. Phys. Lett.*, 2002, **81**, 3058–3060.
208 U. M. Attia, S. Marson and J. R. Alcock, *Microfluid. Nanofluidics*, 2009, **7**, 1.
209 G.-L. Roth, C. Esen and R. Hellmann, *Opt. Express*, 2017, **25**, 18442–18450.
210 J. S. Rossier, M. A. Roberts, R. Ferrigno and H. H. Girault, *Anal. Chem.*, 1999, **71**, 4294–4299.
211 Y. H. Cheng, D. Barpaga, J. A. Soltis, V. Shutthanandan, R. Kargupta, K. S. Han, B. P. McGrail, R. K. Motkuri, S. Basuray and S. Chatterjee, *ACS Appl. Mater. Interfaces*, 2020, **12**, 10503–10514.